

**Analytical model for the radio-frequency sheath**

Uwe Czarnetzki\*

*Institute for Plasma and Atomic Physics, Ruhr University Bochum, 44780 Bochum, Germany*

(Received 20 May 2013; revised manuscript received 1 August 2013; published 3 December 2013)

A simple analytical model for the planar radio-frequency (rf) sheath in capacitive discharges is developed that is based on the assumptions of a step profile for the electron front, charge exchange collisions with constant cross sections, negligible ionization within the sheath, and negligible ion dynamics. The continuity, momentum conservation, and Poisson equations are combined in a single integro-differential equation for the square of the ion drift velocity, the so called sheath equation. Starting from the kinetic Boltzmann equation, special attention is paid to the derivation and the validity of the approximate fluid equation for momentum balance. The integrals in the sheath equation appear in the screening function which considers the relative contribution of the temporal mean of the electron density to the space charge in the sheath. It is shown that the screening function is quite insensitive to variations of the effective sheath parameters. The two parameters defining the solution are the ratios of the maximum sheath extension to the ion mean free path and the Debye length, respectively. A simple general analytic expression for the screening function is introduced. By means of this expression approximate analytical solutions are obtained for the collisionless as well as the highly collisional case that compare well with the exact numerical solution. A simple transition formula allows application to all degrees of collisionality. In addition, the solutions are used to calculate all static and dynamic quantities of the sheath, e.g., the ion density, fields, and currents. Further, the rf Child-Langmuir laws for the collisionless as well as the collisional case are derived. An essential part of the model is the *a priori* knowledge of the wave form of the sheath voltage. This wave form is derived on the basis of a cubic charge-voltage relation for individual sheaths, considering both sheaths and the self-consistent self-bias in a discharge with arbitrary symmetry. The externally applied rf voltage is assumed to be sinusoidal, although the model can be extended to arbitrary wave forms, e.g., for dual-frequency discharges. The model calculates explicitly the cubic correction parameter in the charge-voltage relation for the case of highly asymmetric discharges. It is shown that the cubic correction is generally moderate but more pronounced in the collisionless case. The analytical results are compared to experimental data from the literature obtained by laser electric field measurements of the mean and dynamic fields in the capacitive sheath for various gases and pressures. Very good agreement is found throughout.

DOI: [10.1103/PhysRevE.88.063101](https://doi.org/10.1103/PhysRevE.88.063101)

PACS number(s): 52.25.Dg, 52.25.Fi, 52.27.Aj, 52.80.Pi

**I. INTRODUCTION**

One of the most common methods of plasma generation is to apply a radio-frequency (rf) voltage to two electrodes, typically two parallel planar discs, in a vacuum chamber filled with a certain gas or gas mixtures at low pressures. While one electrode is connected to the rf power supply via a matching network, the other electrode is either the grounded wall or a second electrode of similar size, typically in a plan-parallel configuration. The matching network usually contains a capacitor in series with the discharge that prohibits any dc current. This kind of capacitively coupled plasma (CCP) has found wide application in industry, i.e., for etching of nanostructures in semiconductors or deposition of thin films as in solar-cell manufacturing. The physics of these discharges is strongly dominated by the nonlinear dynamics of the space-charge sheaths that develop in front of the electrodes [1,2].

Numerous investigations have studied the sheath dynamics either experimentally or theoretically [e.g., [3–66]]. In particular, the effect of the dynamics on the formation of ion energy distributions at the surface and nonlocal heating of the electrons has found special interest. Simulations, based on either Particle-in-Cell/Monte-Carlo (PIC/MC) or fluid

models, have strongly contributed to the understanding of the underlying mechanism. Analytical models have often concentrated on certain aspects, e.g., nonlocal (stochastic) heating of electrons or the shape of the ion energy distribution. For these purposes strongly simplified analytical model systems have been constructed or in other cases more advanced analytical models are solved analytically up to a certain point where, from then on, numerical techniques are applied for solving differential equations or evaluating infinite sums. Only few attempts have been made to describe the sheath dynamics fully analytically. The most prominent examples are the Godyak-Sternberg [19] and the Lieberman models [11–13].

In a fluid dynamic picture, the dynamics of the sheaths is described by the continuity and momentum balance equation for ions, Poisson's equation for connecting the field with the space charge, and the Boltzmann factor for the electron density. The light electrons are basically instantaneously in equilibrium with the applied voltage while the heavy ions, at sufficiently high inertia and radio frequencies, react only to the temporal mean field. This leads to a monotonously decreasing ion density from the bulk towards the electrode and an oscillating electron front. When the sheath voltage reaches its minimum, electrons fill almost the entire sheath and the space charge is very small. At the maximum voltage the electrons are basically repelled from the sheath and a large positive space charge develops.

\*uwe.czarnetzki@ep5.rub.de

Although this dynamic behavior is qualitatively rather obvious, a quantitative theoretical description of the sheath dynamics is quite challenging. First, the voltage from the power supply is divided between the two sheaths, the bulk, and the so called series or blocking capacitor, which is usually an integral part of the impedance matching unit between the power supply and the discharge. For asymmetric conditions at the two sheaths, e.g., a small electrode in a chamber with a large wall area, a dc voltage, the so called self-bias, develops across the discharge. This is possible because the same dc voltage, but with the opposite sign, is established across the series capacitor. This self-bias is a consequence of the interaction between the two sheaths and the blocking of any dc current by the series capacitor. While for a single frequency discharge the applied voltage wave form is usually sinusoidal, this is not necessarily the case for the individual sheath voltages. Second, heavy ions respond only to the time averaged field in the sheath. This field is determined by Poisson's equation, which requires knowledge of the temporal average of the electron density. However, this average can only be calculated if the dynamic of the electron density is known. As a consequence, iterative integration techniques are usually applied in order to solve the coupled system of equations.

Godyak and Sternberg [19], as well as Lieberman, have avoided these difficulties by considering an isolated sheath with a known sinusoidal current wave form [11,12]. The spatial electron density distribution is simplified by a step profile. Further, the equations are solved analytically for the case of negligible collisionality, i.e., ions do not interact with the neutral gas background. A collisional extension of the model is solved numerically by Godyak and Sternberg [19] and analytically under certain assumptions by Lieberman [12] and also Vallinger *et al.* [15]. These models have greatly contributed to the understanding of the rf sheath dynamics and, in particular, Kawamura *et al.* have applied his model successfully to calculating stochastic electron heating [55]. Brinkman has developed a more advanced fluid model that requires knowledge of the sheath voltage instead of the current and takes into account also ion-neutral collisions [46,47]. Further, a realistic spatial electron distribution is included. However, the model is only half analytical and requires iterative numerical solution. Similarly, Riemann and Biehler have performed in depth kinetic studies using the Boltzmann equation with particular focus on the ion energy distribution but again need numerical techniques for integration of the differential equations in the end [9,10]. Most recently Chabert and Turner have proposed a novel fully analytical model for the collisionless sheath where they demonstrate that the fluid equations can be integrated easily if the mean electron density is assumed as a constant fraction of the ion density [44]. This ignores the strong spatial variation of the fractional electron density. Further, like in the Lieberman model, the ion density diverges at maximum sheath extension. Another recent model is proposed by Elgendy *et al.* [67], which is an analytical approximation to the half-analytical Brinkmann model for the collisionless as well as the collisional sheath [46,47]. Both novel analytical models are again based on a known current wave form.

Here a novel approach is introduced that provides simple analytical expressions for all sheath quantities. The model

is based on the applied rf voltage wave form and not the current. The applied voltage wave form is separated into two individual sheath voltage wave forms and the self-bias on the basis of a cubic charge-voltage relation for the sheaths. The first two moments of the Boltzmann equation and Poisson's equation are combined in a single integro-differential equation, the sheath equation. This equation contains as a key quantity the screening function that describes the screening of the positive ion space charge in the sheath by the time averaged electron charge. This function is approximated by Chabert and Turner in their work [44] as a constant but here the full spatial variation is considered. The sheath equation has two control parameters representing the ion collisionality in the sheath and the Debye length at the sheath edge. In addition, the maximum sheath extension is used as normalization length. The equation is solved numerically and analytically using certain approximations. Comparison of the analytical results with iterative numerical solutions of the sheath equation and experimental data from the literature show excellent agreement. The model presented in this work offers opportunities for either further investigations of the sheath physics, e.g., determination of ion energy distribution functions or stochastic electron heating, or incorporating it in multidimensional fluid dynamic simulation codes, which often do not resolve the sheath and require some sheath model linked to the boundary.

The remaining part of the paper is organized as follows.

First, the basic differential equation for the ion drift velocity is derived (Sec. II A). Boundary conditions are discussed in Sec. II B. In order to enhance readability of the main text, proofs of certain assumptions made in the model are moved to an appendix. In particular, in Appendix A the derivation of an approximate momentum balance equation and the error caused by the underlying assumptions are discussed in comparison to the exact kinetic solution for a linear electric field. The derivation of a sinusoidal sheath voltage for discharges of various symmetries and with an applied sinusoidal single-frequency rf voltage is presented in Appendix B. The sheath differential equation is solved numerically in Sec. II C. Details on determining a universal form for the screening function are mostly moved to Appendix C. In Sec. II D further important sheath quantities are calculated from a known solution for the ion drift velocity, e.g., the spatial ion density profile, the dynamic space charge, or the time averaged and dynamic voltages and electric fields. Subsequently, the Child-Langmuir laws, i.e., the relation between the time averaged sheath voltage and current, are derived separately for the collisionless case as well as the collisional case (Sec. II E). In the final two sections (Secs. II F and II G) approximate analytical solutions for the collisionless case as well as the collisional case are derived. Some key integrals are solved approximately in Appendix D. The numerical and analytical solutions are compared and the results are discussed in Sec. III for the collisionless case as well as the collisional case (Sec. III A). A simple transition formula connects these extremes (Sec. III B). Section III is closed with a comparison of the analytical model with experimental data from the literature on time averaged and time resolved sheath electric fields (Sec. III C). Finally, the results are summarized and an outlook on further tests, extensions, and applications of the model is given (Sec. IV).

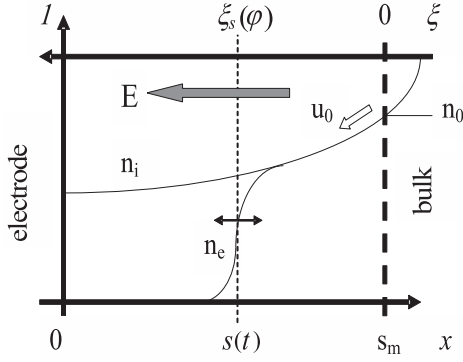


FIG. 1. Basic scheme of the density profiles in the sheath, including notations and coordinate systems used in the model. Details are explained in the text.

## II. DERIVATION OF THE RF SHEATH MODEL

### A. The basic rf sheath equation

The model for a planar rf sheath is based on the following simplifying assumptions.

(a) Ions are massive enough to respond only to the time averaged sheath electric field. ( $\omega \gg \omega_{pi}$ , where  $\omega$  is the (fundamental) rf angular frequency and  $\omega_{pi}$  is the mean ion plasma frequency).

(b) Ions in the sheath undergo only charge exchange collisions.

(c) These collisions take place with a constant cross section  $\sigma$  or mean free path  $\lambda$ .

(d) The electron density distribution can be represented by a step function (Fig. 1).

(e) The sheath potential becomes zero at the time of the sheath collapse.

(f) Ionization within the sheath is neglected.

These assumptions are quite standard and have been discussed in the literature before [17,35,57,61]. Certainly, the neglect of elastic collisions (b) and the assumption of a constant cross section for charge exchange (c) are introducing some error. The strongest deviation can be expected at low energies near the sheath edge, where the cross section is changing rather strongly. The step profile in (d) is defined by the condition that the number of electrons beyond the step position equals the integral difference between the ion and electrons densities on the other side [19,29,33,51]. The approximation is naturally precise for the calculation of the total space charge but introduces an error around the temporary sheath edge when applied to calculating the electric field or the voltage, in particular at the extremes. The extension of the electron density around the temporary sheath edge position is determined by the electron temperature  $T_e$ . In this sense, the step profile represents the limiting case of zero electron temperature. Consistently, this limiting case is also applied to the minimum potential at the time of the sheath collapse (e). The step model has also consequences for the boundary condition for the oscillating field at the point of the instantaneous sheath edge as well as for time averaged field at the point of maximum sheath extension. This is discussed in detail the subsequent Secs. II B and II D. Ionization in the sheath can be neglected at low pressures (f) but at higher

pressures secondary electrons can ionize and multiply within the sheath. This limits the upper pressure range to typically  $p < 100$  Pa. The convenient consequence of this assumption is conservation of the ion flux within the sheath.

Essential for the model of a planar sheath is the one-dimensional momentum balance equation for ions with charge exchange collisions. This fluid equation is effectively a first order differential equation for the square of the drift velocity  $W = u^2/u_0^2$ , where  $u_0$  is the drift velocity by which ions enter the sheath at its maximum temporal extension  $s_m$ :

$$W' + \beta W = \bar{F}(\xi), \quad W(\xi = 0) = 1. \quad (1)$$

Here  $\bar{F}(\xi) = \bar{E}(\xi)/E_0$  is the normalized time averaged electric field with  $E_0 = m_i u_0^2 / (2es_m)$ , where  $m_i$  is the ion mass. Physically,  $E_0$  is the homogeneous field necessary to accelerate in free fall an ion initially at rest over the full length of the sheath to its initial velocity  $u_0$ . Therefore, the time averaged electric field in the sheath  $\bar{E}(\xi)$  is much larger except very close to the maximum sheath extension where the field vanishes. The parameter  $\beta = \pi s_m / \lambda$  counts the average number of collisions in the sheath and is therefore a measure of the collisionality. Equation (1) is not exact but an approximation to the first moment of the corresponding Boltzmann equation. Derivation of this equation and the accuracy of the approximation are discussed in detail in Appendix A. Unless stated otherwise the coordinate system used in the calculation has its zero position at the maximum sheath extension and the length scale is normalized to this value as shown in Fig. 1 ( $\xi = 1 - x/s_m$ , i.e.,  $0 \leq \xi \leq 1$ ). In this coordinate system, the electric field is always pointing in the direction of increasing  $\xi$ .

This equation can now be differentiated once in order to combine it with Poisson's equation via the derivative of the time averaged electric field. Poisson's equation for the time averaged field reads

$$\frac{\partial \bar{F}}{\partial \xi} = \frac{es_m}{E_0 \epsilon_0} (n_i - \bar{n}_e). \quad (2)$$

The electron density is given in the frame of the step model by the ion density  $n_i$  and the Heaviside function  $\theta$ :

$$n_e(\xi, t) = n_i(\xi) \theta[\xi_s(\varphi) - \xi]. \quad (3)$$

Here  $\xi_s(\varphi)$  is the momentary sheath edge which varies with the rf phase  $\varphi = \omega t$ . The integral for the time average can now be carried out directly. However, care has to be taken about the monotonous intervals of the sheath voltage wave form. In case of a single rf, the integral can be limited to one half of the rf period. For multifrequency discharges the average has to be carried out over multiple subintervals. Now the integral average of the electron density becomes

$$\bar{n}_e = n_i(\xi) \frac{1}{\pi} \int_0^\pi \theta[\xi_s(\varphi) - \xi] d\varphi = n_i(\xi) \frac{\varphi(\xi)}{\pi}. \quad (4)$$

The relation  $\varphi(\xi)$  can be obtained by integrating Poisson's equation twice over the entire sheath and combining this with the *a priori* known temporal form of the sheath voltage. In the following, the case of a single frequency rf discharge is considered where the sheath voltage  $V_s$  can be represented by a certain power  $k$  of a sinus function, i.e.,  $V_s = \hat{V} |\sin(\varphi/2)|^k$ . The sheath voltage wave form and the justification for this particular wave form are discussed in more detail in

Appendix B in connection with the charge-voltage relation of the sheath. In case of an infinitely asymmetric discharge, where the self-bias equals the amplitude of the applied rf voltage  $V_0$ , one finds  $k = 2$  and  $\hat{V} = 2V_0$ . On the other hand, for symmetric discharges, where the self-bias vanishes, the sheath voltage can be well approximated by a power of  $k \approx 3$  and  $\hat{V} = V_0$ . The fact that the model assumes knowledge of the sheath voltage makes it quite distinct from the Lieberman or the Godyak/Sternberg models where knowledge of the current wave form is assumed.

The sheath voltage is obtained by integrating Poisson's equation twice and applying a partial integration in order to remove one of the two integrals:

$$\hat{V} \sin^k\left(\frac{\varphi}{2}\right) = \frac{e s_m^2}{\epsilon_0} \int_{\xi}^1 (1 - \xi') n_i(\xi') d\xi'. \quad (5)$$

Obviously, the extreme values are related in the following way:

$$\hat{V} = \frac{e s_m^2}{\epsilon_0} \int_0^1 (1 - \xi') n_i(\xi') d\xi'. \quad (6)$$

Further, at this point it is useful to replace the ion density by the velocity variable  $W$  using the continuity equation ( $n = n_i/n_0 = 1/\sqrt{W}$ , where  $n_0$  is the ion density at  $s_m$ ). Now by combining Eq. (6) with Eq. (5) one can solve for  $\varphi$ , which determines the average electron density in Eq. (4). By taking the derivative of Eq. (1) and combining it with Eqs. (2) and (4), a single compact equation for the square of the ion drift velocity can now be formulated:

$$W''(\xi) + \beta W'(\xi) = \gamma^2 \frac{g(\xi)}{\sqrt{W(\xi)}}, \quad (7)$$

where  $g/\sqrt{W}$  represents the normalized space charge. The screening function  $g(\xi) = 1 - \bar{n}_e/n_i$  describes the screening of the ion density in the sheath by the time averaged electron density:

$$g(\xi) = \frac{2}{\pi} \arccos \left\{ \left[ 1 - \frac{\int_0^{\xi} \frac{1-\xi'}{\sqrt{W(\xi')}} d\xi'}{\int_0^1 \frac{1-\xi'}{\sqrt{W(\xi')}} d\xi'} \right]^{1/k} \right\}. \quad (8)$$

In the final step use has been made of the relation  $\pi/2 - \arcsin(x) = \arccos(x)$ . Obviously,  $g(0) = 0$ , i.e., at the position of maximum sheath extension where quasineutrality holds, and  $g(1) = 1$ , i.e., at the electrode where the electron front resides only for an instance. Between these extremes a smooth and monotonous transition is made. Equation (7) depends on two dimensionless parameters:

$$\beta = \pi \frac{s_m}{\lambda} \quad \text{and} \quad \gamma = \frac{\sqrt{2}}{c} \frac{s_m}{\lambda_D}. \quad (9)$$

Here  $\lambda_D = \sqrt{\epsilon_0 k T_e / (e^2 n_0)}$  is the Debye length at the maximum sheath extension and  $c = u_0/u_B$ .  $u_B = \sqrt{k T_e / m_i}$  is the Bohm velocity and  $k$  the Boltzmann constant. It should be noted that the introduction of the Debye length and the electron temperature is not a necessity as  $\gamma$  can also be expressed directly by  $u_0$  and the other parameters. However, in this way the physical meaning of  $\gamma$  becomes more obvious. While  $\beta$  represents the collisionality of the sheath, i.e., the pressure dependence,  $\gamma$  represents the plasma density dependence, i.e.,

rf power dependence. The factor  $c$  considers the fact that the velocity by which ions enter the sheath at the maximum sheath extension is not necessarily identical to the classical Bohm velocity. When ion-neutral collisions become important  $c < 1$  will apply. Effectively, the factor  $c^2 k T_e$  is a single parameter in the model.

A typical parameter range for the collision parameter is  $0 \leq \beta \leq 30$ . The lower limit corresponds to the collisionless sheath at very low pressure. The upper limit is given by the increasing role of ionizing collisions by secondary electrons within the sheath at higher pressures (typically at  $p > 50\text{--}100$  Pa). Typical values for the density parameter are in the range  $15 < \gamma < 100$ . The lower limit is set by the fact that already a sheath at the dc floating potential has about  $s_m/\lambda_D \approx 10$ . The upper limit can be found by arguing that a characteristic Debye length is about  $\lambda_D \approx 0.1$  mm and the sheath extension will rarely exceed about  $s_m = 7$  mm. For fixed values for  $u_0$  and  $s_m$ , the proposed range for  $\gamma$  corresponds to a density variation by already more than a factor of 40. Variation of the sheath width with the density extends the density range effectively to about a factor 100. For low-pressure discharges  $\lambda_D \ll \lambda$  applies, which is equivalent to  $\beta \ll \gamma$ .

Although the basic rf sheath equation (7) has a very compact form, it cannot be integrated analytically. Even numerical integration can only be performed iteratively since the screening function  $g$  contains an integral over  $W$  which extends over the entire sheath length; i.e., the solution needs to be known in order to carry out the integral.

## B. Boundary conditions

Equation (7) is a second order equation but only one boundary condition,  $W(0) = 1$ , has been specified so far. The value of  $W'(0)$  relates to the electric field at the boundary by Eq. (1). Therefore, the correct boundary condition results from a full discharge model combining the sheath with the bulk plasma and taking into account also changes in the ion mobility. In particular, an entirely self-consistent boundary condition would require including the real spatial profile of the electron front. As a consequent of the step model with vanishing space charge at the maximum sheath extension the right hand side of Eq. (7) is zero at the boundary. Consequently,  $W''(0) = -\beta W'(0) \leq 0$  follows. For any  $\beta > 0$  this is inconsistent since  $W'' \geq 0$  should apply at the sheath edge. However, a systematic expansion shows that the right hand side of Eq. (7) increases in the vicinity of the boundary like  $\sqrt{\xi}$  so that the sign of the curvature changes to positive almost immediately. Using the expansion and the boundary condition defined below, one can identify the turning point of the curvature at  $\xi_c \approx 0.62\tilde{v}(1)(\beta/\gamma)^2 \approx 0.4(\lambda_D/\lambda)^2 \ll 1$ , with  $\tilde{v}(1) \approx 0.1 - 0.2$  defined below by Eq. (17). In agreement with numerical solutions typical values for  $\xi_c$  are in the range  $10^{-3}$  to  $10^{-2}$ . In conclusion, the differential equation automatically corrects the error on a very short length scale so that the initial inconsistency does not really matter. Constructing, however, a fully self-consistent boundary condition would require substantial extension of the model. This is not very practical and fortunately not entirely necessary. For a high voltage sheath, the second boundary condition has, in fact, very little influence on the sheath properties further down

into the sheath. For practical purposes it might be sufficient to define a reasonable simple second boundary condition that ensures some basic requirements of the sheath density profile. Therefore, what follows should be viewed rather as a motivation than a derivation.

One has to demand that the ion sheath density decreases smoothly and monotonically. This requires  $n'' \geq 0$ . Expressing again the ion density by  $1/\sqrt{W}$  and making use of Eq. (7) to substitute the second order derivative, one finds

$$W' \geq -\frac{\beta}{3}W + \sqrt{\left(\frac{\beta}{3}W\right)^2 + \frac{2}{3}\gamma^2 \frac{g}{\sqrt{W}}}. \quad (10)$$

In the vicinity of the sheath edge one might still approximate  $W \approx 1$ , while  $g$  must have values in the range  $0 < g < 1$ . Further, considering the possible parameter range discussed above one might neglect the terms containing  $\beta$  in comparison to the term containing  $\gamma$ . This motivates

$$W' \geq \sqrt{\frac{2r}{3}}\gamma. \quad (11)$$

Here  $r$  is a number between 0 and 1. Empirically, one finds  $r = 3/8$  for the entire parameter range of  $\beta$  and  $\gamma$ . Using the minimum value, the approximate form of the second boundary condition becomes  $W'(0) = \gamma/2$ . This corresponds to an initial density gradient of  $n'(0) = -\gamma/4$  or  $\partial n/\partial x = n_0/(2^{3/2}\sqrt{c}\lambda_D)$  or, equivalently, to an ambipolar field proportional to  $kT_e/\lambda_D$ , which has the natural scaling for  $\lambda_D \ll \lambda$  and is also used in the Godyak/Sternberg model [19]. Further, use of the minimum value is equivalent to a vanishing curvature of the density around the sheath edge. Since the curvature is concave in the bulk but convex within the sheath the transition is naturally located here.

Although this second boundary condition is essential for performing the numerical integration of the differential equation, it is actually quite uncritical for the final solution. Numerical tests show that even in the extreme and unrealistic case  $W'(0) = 0$  [corresponding to  $n'(0) = 0$ ] the solutions always relax quickly to the solutions for the above boundary condition over a small fraction of the sheath length. As shown below, the approximate analytical solutions do not depend on this boundary condition but, nevertheless, show very good agreement with the numerical solutions using it.

### C. Numerical solution and the screening function

All numerical calculations in this work are carried out by using the commercial software MATHEMATICA. This includes the numerical integration of the differential equation as well as solution of certain integrals defined in the following section.

In the following only the case of a fully asymmetric discharge is investigated, i.e., a discharge setup where the grounded area is much larger than the powered electrode area. In this case the sheath voltage is represented exactly by  $k = 2$  (Appendix B). The sheath equation can now be solved iteratively. Initially the screening function  $g$  is specified by setting in the integral  $W = W^{(0)} = 1$ , i.e., assuming a constant ion density in the sheath. This rather drastic initial assumption

yields then

$$g^{(0)}(\xi) = \frac{2}{\pi} \arccos(1 - \xi). \quad (12)$$

With this initial form  $g^{(0)}(\xi)$  now the differential equation (7) can be integrated to yield a first order solution  $W^{(1)}(\xi)$ . This solution can then be used in the integrals in order to calculate an improved form of the screening function  $g^{(1)}(\xi)$ , which again leads to an improved solution  $W^{(2)}(\xi)$  and so forth. Convergence is very fast and the final form of  $g$  does not deviate very strongly from the simple initial form. For any choice of parameter combinations there is no noticeable difference between the first order form of  $g^{(1)}$  and the following higher orders  $g^{(j>1)}$ . Correspondingly, there is no significant difference between the second order solution of  $W$  and any higher orders. A typical example is shown in Fig. 2. The root-mean-square average  $\sigma$  for the relative deviation of  $g^{(j)}$  and  $W^{(j)}$  from the infinite solution ( $j \rightarrow \infty$ , where  $j$  is the number of iterations) shrinks exponentially with the same exponent. In the above example it is  $\sigma = 0.107 \times 0.044^{j-1}$  for  $W^{(j)}$ , where  $j$  is the number of iteration, i.e.,  $\sigma = 4.7 \times 10^{-3}$  in second order. These numbers vary little for the entire parameter range of  $\gamma$  and  $\beta$ .

Further, the particular form of  $g$  depends only very weakly on the choice of the governing parameters  $\beta$  and  $\gamma$  (Fig. 3). A

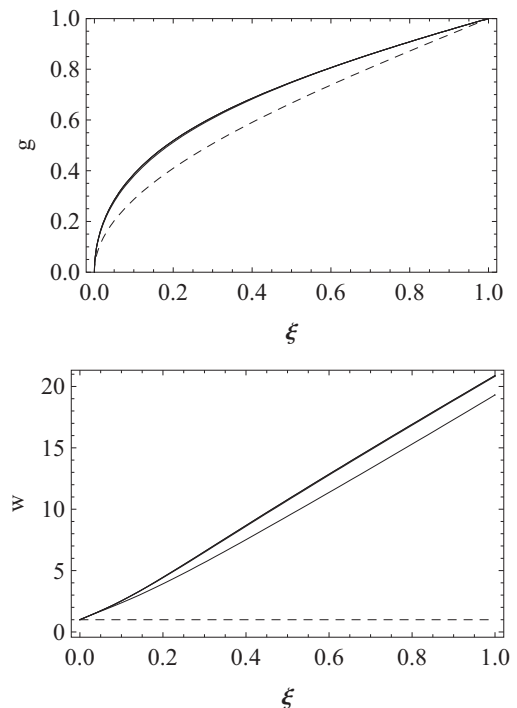


FIG. 2. Numerical iteration of the differential equation for the rf sheath ( $\beta = 10$ ,  $\gamma = 30$ ) using five iteration steps (top, screening function  $g$ ; bottom, normalized square of the ion drift velocity  $W$ ). The initial forms  $g^{(0)}$  and  $W^{(0)}$  by which the iteration starts are indicated by the dashed lines. All subsequent solutions of  $g^{(j>0)}$  are effectively on top of each other. Only for  $W$  can the first order solution  $W^{(1)}$  be identified as a separate curve but already the second and all higher orders  $W^{(j>1)}$  are also all on top of each other.

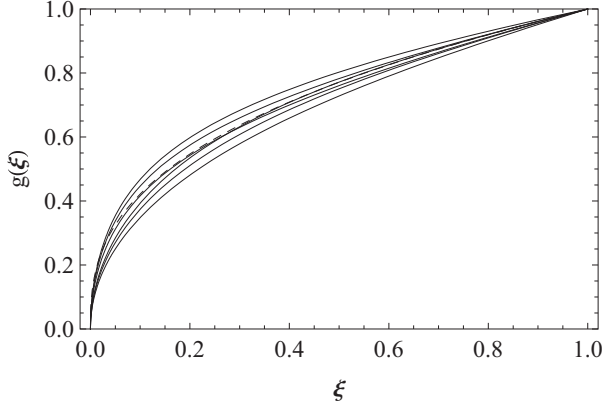


FIG. 3. Comparison of the approximate analytical form of the screening function  $g_a$  (dashed line) and exact numerical solutions (solid lines) for combinations of two values of the density parameter ( $\gamma = 15$  and  $50$ ) and three values of the collision parameter ( $\beta = 0, 3, \text{ and } 10$ ): (a)  $\beta = 0, \gamma = 15$ , (b)  $\beta = 0, \gamma = 50$ , (c)  $\beta = 3, \gamma = 15$ , (d)  $\beta = 3, \gamma = 50$ , (e)  $\beta = 10, \gamma = 15$ , (f)  $\beta = 10, \gamma = 50$ . The order is from bottom to top: (e), (c), (a), (f), (d), (b).

reasonable universal approximation is found in Appendix C:

$$g(\xi) \approx g_a(\xi) = \xi^\nu \approx \xi^{3/8}. \quad (13)$$

The empirical power law is motivated by the approximate behavior of the initial form of  $g$  as given by the right hand side of Eq. (12). This choice of  $g_a$  is compared to the exact self-consistent numerical solution for various parameter combinations in Fig. 3. The lower value of  $\gamma = 15$  corresponds to an extremely low rf voltage (sheath width of only  $10 \lambda_D$ ). Here the collisionless case is on top of  $g_a$  and the difference increases with collisionality, i.e., increasing  $\beta$ . The high value of  $\gamma = 50$  is more typical (sheath width of  $35 \lambda_D$ ). There the collisionless case shows the strongest deviation while the highly collisional case is basically on top of  $g_a$ . One can conclude that increasing  $\beta$  shifts the curves downwards (higher effective exponent) and increasing  $\gamma$  has the opposite effect (lower effective exponent). Therefore, the choice made here for the universal analytical form  $g_a$  is a compromise that provides a reasonable approximation within a wide parameter range.

In Appendix C it is shown how generally an optimized exponent  $\nu$  can be found from the numerical result for  $g$ . With this optimized exponent excellent agreement with the original form of  $g$  is achieved. Depending on  $\gamma$  and  $\beta$ , the optimized values for  $\nu$  vary only within a narrow range and the universal average value of  $\nu = 3/8$  is reasonably chosen; i.e., the actual variation of  $\nu$  around this value has little effect on the final result.

Naturally, using  $g_a$  as the starting configuration in the iteration leads to a correspondingly faster convergence and even smaller deviations between the first and the higher order solutions for  $W$ . With very good accuracy one can now even avoid the inconvenient iteration procedure and integrate the differential equation directly. Within the parameter range defined above the relative differences are only few percent. However, the main use of  $g_a$  in this work is for obtaining approximate analytical solutions as shown below.

#### D. Calculation of further quantities

Once a solution for  $W$  is found, other quantities can be calculated in a straightforward manner. Naturally, the normalized ion density [ $n(0) = 1$ ] is given by  $n = 1/\sqrt{W}$ . The normalized space charge  $0 \leq q \leq 1$  in the sheath [normalized to  $Q_0 = en_0 s_m \tilde{q}(1)$ ] as function of the position of the temporary sheath edge is given by

$$q(\xi) = 1 - \frac{\tilde{q}(\xi)}{\tilde{q}(1)}, \quad (14)$$

with

$$\tilde{q}(\xi) = \int_0^\xi \frac{d\xi'}{\sqrt{W(\xi')}}. \quad (15)$$

The normalized sheath voltage  $0 \leq v \leq 1$  [normalized to  $V_0 = en_0 s_m^2 \tilde{v}(1)/\epsilon_0 = \gamma^2 E_0 s_m / c^2 \tilde{v}(1)$ ] is

$$v(\xi) = 1 - \frac{\tilde{v}(\xi)}{\tilde{v}(1)}, \quad (16)$$

with

$$\tilde{v}(\xi) = \int_0^\xi \frac{1 - \xi'}{\sqrt{W(\xi')}} d\xi'. \quad (17)$$

The two functions  $\tilde{q}(\xi)$  and  $\tilde{v}(\xi)$  are called the charge function and the voltage function, respectively. With these definitions the screening function becomes

$$g(\xi) = \frac{2}{\pi} \arccos[\sqrt{v(\xi)}]. \quad (18)$$

The normalized mean electric field is given by Eq. (1). This brings back naturally the question of boundary conditions since Eq. (1) implies that the time averaged field at maximum sheath extension is defined by  $\bar{F}(0) = \beta W(0) + W'(0) \neq 0$ . However, the actual value might, in fact, be quite different since here, first, the finite extension of the electron front leaves a finite space charge and, second, the acceleration of ions to the Bohm speed is actually a quite complicate process. For instance, Riemann calculates for the dc collisional case an electric field at the Bohm point of  $F_B = 0.88\beta^{3/5}\gamma^{2/5}$  (using the present normalization) [49,50]. On the other hand, Brinkman shows that the Bohm point moves into the sheath at high collisionality so that it becomes unrelated from the start of the space-charge region [64]. This means the point of maximum sheath extension as defined in this model is not necessarily the Bohm point, as discussed already above. Anyway, it is not the intention of this work to engage in the discussion of quantities at the Bohm point and the step model is, in fact, badly suited to do so. Since the field at the edge is substantially smaller than the fields within the sheath here the field at the temporary sheath edge and consequently also the value for the temporarily averaged field at the point of maximum sheath extension is set simply to zero. Therefore, the small actual value of the field at the edge, in reality, is ignored. In conclusion, the time averaged field is determined by integrating either the left hand side or the right hand side of Eq. (7) from zero to a point  $\xi$  within the sheath. Clearly, the question of the detailed quantitative values of the ion velocity and the field at the boundary is an aspect that could be improved further. However, such investigation would go well beyond the

scope of this work and also the limitations of the simplified model presented here.

Now the dynamic electric field in the sheath for  $\xi \geq \xi_s$  can be expressed as follows:

$$F(\xi, \xi_s) = \gamma^2 [\tilde{q}(\xi) - \tilde{q}(\xi_s)]. \quad (19)$$

Apparently, the maximum field is found at the electrode and the field strength is generally increased with  $\xi_s$  approaching zero, i.e., expanding sheath extension. The absolute maximum field strength is  $\gamma^2 \tilde{q}(1)$ . The functional relation between the sheath edge position and the rf phase is determined in the following.

The normalized sheath voltage can be approximated by a cubic charge-voltage relation [Appendix B, Eq. (B5)]:

$$v(q) = q^2 + (a - 1)q^2(1 - q). \quad (20)$$

$$q(v) = \frac{a}{3(a - 1)} \left[ 1 - 2\cos \left( \frac{1}{3} \left\{ \arccos \left[ 1 - \frac{27(a - 1)^2}{2a^3} v(\varphi) \right] + \pi \right\} \right) \right]. \quad (22)$$

Differentiation of Eq. (22) with respect to  $\varphi$  gives the normalized displacement current density  $j$  [normalized to  $j_0 = en_0 s_m \omega \tilde{q}(1)$ ]:

$$j(\varphi) = \frac{3(a - 1) \sin \left( \frac{1}{3} \left\{ \arccos \left[ 1 - \frac{27(a - 1)^2}{2a^3} \sin^2 \left( \frac{\varphi}{2} \right) \right] + \pi \right\} \right) \sin(\varphi)}{2a^2 \sqrt{1 - \left[ 1 - \frac{27(a - 1)^2}{2a^3} \sin^2 \left( \frac{\varphi}{2} \right) \right]^2}}. \quad (23)$$

However, the displacement current density can also be determined exactly in a parametric representation without using the cubic charge-voltage relation:

$$j(\xi_s) = \frac{\partial q}{\partial \varphi} = \frac{\frac{\partial q}{\partial \xi} \partial v}{\frac{\partial v}{\partial \xi} \partial \varphi} = \frac{\tilde{v}(1) \sqrt{v(\xi_s)[1 - v(\xi_s)]}}{\tilde{q}(1) (1 - \xi_s)}. \quad (24)$$

The rf phase  $\varphi$  is related to the dynamic sheath edge position  $\xi_s$  via the sheath voltage:

$$\varphi(\xi_s) = 2\arcsin[\sqrt{v(\xi_s)}]. \quad (25)$$

In this way a parametric presentation of the displacement current as a function of the rf phase is possible by varying the dynamic sheath edge position between zero and one. Further, symmetry can be applied to extend the range from the first half cycle  $0 \leq \varphi \leq \pi$  to the entire period  $0 \leq \varphi \leq 2\pi$ , i.e.,  $j(\varphi) = -j(2\pi - \varphi)$ . This presentation is particularly useful in order to calculate the current density without making approximations and can be applied to the numerical as well as the analytical solution of the sheath equation. If the sheath edge position as a function of the rf phase is known, Eq. (24) becomes even an explicit expression for the current:

$$j(\varphi) = \frac{1}{2(3 - a)} \frac{\sin(\varphi)}{1 - \xi_s(\varphi)}. \quad (26)$$

Here the explicit form of the sheath voltage is used and the ratio  $\tilde{v}(1)/\tilde{q}(1)$  is replaced with the cubic correction parameter [Eq. (21)]. However, even for the analytical solutions presented below, deriving an exact analytical expression for  $\xi_s(\varphi)$  is not possible. Instead, an approximate relation for  $\xi_s(q)$  is introduced in Appendix D, where the cubic charge-voltage relation provides  $q(v)$  via Eq. (22). Finally, the known sheath

The relation is dominated by the quadratic term and the cubic correction parameter  $a$  is given by [Appendix B, Eq. (B7)]:

$$a = 3 - \frac{\tilde{q}(1)}{\tilde{v}(1)}. \quad (21)$$

It is shown in Appendix B that the cubic correction parameter accounts for the spatial inhomogeneity of the ion density within the sheath. The parameter can range between 1 for a homogenous ion density profile and 2 for an infinitely steep profile.

Inversion of the cubic equation (20) provides  $q(v)$ , where the normalized sheath voltage wave form  $v(\varphi)$  is again assumed to be a known function of the rf phase  $\varphi = \omega t$ . Since Eq. (20) has only a single real root, the relevant solution is

voltage is  $v = \sin^2(\varphi/2)$  so that this closes the chain to obtain  $\xi_s(\varphi)$ . The approximate expression for  $\xi_s(q)$  are discussed further in Secs. II F and II G in connection with the analytical solutions.

The relation  $\xi_s(\varphi)$  is also important for calculating the temporally and spatially resolved dynamic electric field in the sheath. Last, but not least, the sheath edge velocity can be deduced by differentiating  $\xi_s$  with respect to  $\varphi$ . From the definition of the normalized sheath voltage, one finds  $\partial \xi_s / \partial \varphi = -\partial v / \partial \varphi \tilde{v}(1) \sqrt{W(\xi_s)} / (1 - \xi_s) = \mp \sqrt{v(1 - v)} \tilde{v}(1) \sqrt{W(\xi_s)} / (1 - \xi_s)$ , where the latter sign depends on whether the sheath is expanding or contracting. This velocity is the essential parameter for the stochastic heating of electrons [46,53–56,60].

In summary, all static and dynamic sheath quantities can be derived analytically once the solution for  $W(\xi)$  has been determined. In addition to the above quantities, also a relation between the temporal means of the sheath voltage and the current density, i.e., the ion current density, can be derived. Such a relation is generally known as the rf equivalent to the Child-Langmuir law, originally derived in the dc case for space charge limited currents in tubes [1,2]. The rf Child-Langmuir laws for the collisionless as well as the collisional case are derived in the following section.

### E. The rf Child-Langmuir law

The normalized mean sheath voltage (normalized to  $V_0 = E_0 s_m$ ) is found by integrating Eq. (1):

$$\bar{v} = W(1) - 1 - W'(0) + \beta \left[ \int_0^1 W(\xi) d\xi - 1 \right]. \quad (27)$$

This relation can be used to construct the rf equivalent to the Child-Langmuir law. This generally means the relation between the mean current density, i.e., the ion current density  $\bar{j} = en_0 u_0$ , and the mean sheath voltage  $\bar{V}$  (the capital letter indicates the non-normalized value). In particular for the extreme cases of the collisionless sheath ( $\beta = 0$ ) and the highly collisional sheath ( $\beta \gg 1$ ) this can be carried out in a simple way.

For the collisionless case, Eq. (7) needs to be integrated twice in order to calculate the voltage, where one of the two integrations can again be carried out by using partial integration:

$$\begin{aligned} \bar{v} = W(1) - 1 - W'(0) &= \gamma^2 \int_0^1 \frac{(1-\xi)g(\xi)}{\sqrt{W(\xi)}} d\xi \\ &= \left[ \frac{\gamma^2}{p_1(\gamma)} \right]^{2/3}. \end{aligned} \quad (28)$$

The definition of  $p_1$  is motivated by the fact that Eq. (7) indicates that  $\sqrt{W} \propto \gamma^{2/3}$  so that  $p_1$  can be expected to vary only weakly with  $\gamma$ :

$$\begin{aligned} p_1(\gamma) &= \left( \int_0^1 \frac{\gamma^{2/3}(1-\xi)g(\xi)}{\sqrt{W(\xi)}} d\xi \right)^{-3/2} \\ &= \frac{\gamma^2}{[W(1) - 1 - W'(0)]^{3/2}}. \end{aligned} \quad (29)$$

For an exact solution of the sheath differential equation (7) both alternative definitions are exactly identical and the right hand side is clearly the simpler form for evaluation. However, this identity does not necessarily apply to an approximate solution which is derived in the subsequent section. Both alternatives, the integral and the direct calculation, are compared at the end of Sec. III A.

Returning now to non-normalized values and rearranging Eq. (28) gives directly the Child-Langmuir law:

$$\bar{j} = p_1(\gamma) \varepsilon_0 \sqrt{\frac{2e}{m}} \frac{\bar{V}^{3/2}}{s_m^2}. \quad (30)$$

The numerical value of  $p_1$  can be determined from either the numerical solution or the analytical approximation given in Sec. II F. As shown in Sec. III A,  $p_1$  decreases in fact with  $\gamma$  and varies within the relevant parameter range between 1.6 and 1.0. For very large values  $p_1$  converges to  $133/142 = 0.94$ . A reasonable average value is  $p_1 = 1.2$ , which is found for  $\gamma = 40$ . This is significantly larger than the factor of 0.82 obtained by Lieberman [11]. However, Lieberman's calculation is based on the assumption of a sinusoidal current and not a sinusoidal voltage, which might explain the difference.

In case of high collisionality, a function  $p_2(\gamma, \beta) = p_1(\gamma, \beta) \sqrt{\beta}/2$  can be defined if the integral definition for  $p_1$  is used:

$$p_2(\gamma, \beta) = \left[ \int_0^1 \left( \frac{4\gamma^2}{\beta} \right)^{1/3} \frac{(1-\xi)g(\xi)}{\sqrt{W(\xi)}} d\xi \right]^{-3/2}. \quad (31)$$

Alternatively, one could also in this case use integration of the right hand side of Eq. (7) but this leads to an additional integral over  $W$ , which is not necessarily easier to solve. By neglecting terms not containing  $\beta \gg 1$  in Eqs. (8) and using the universal

expression for the screening function  $g \approx g_a = \xi^{3/8}$ , one can integrate easily for  $W$  and insert the result in Eq. (31):

$$p_2(\gamma, \beta) \approx \sqrt{\frac{11}{3}} \left[ \int_0^1 \frac{(1-\xi)\xi^{3/8}}{\left( \frac{11\beta}{12\gamma^2} + \xi^{11/8} \right)^{1/3}} d\xi \right]^{-3/2}. \quad (32)$$

For very large values  $\gamma^2/\beta$  one can reasonably neglect the first term in the denominator. Then the integral becomes trivial and independent of all parameters. This is actually the motivation for the particular definition of  $p_2$ . The asymptotic value of  $p_2 = \sqrt{23/3} \cdot 253/576 \approx 1.2$  is effectively identical to the average value for the collisionless case. However, generally also  $p_2$  is not a constant but can be expected to vary weakly with the control parameters by the ratio  $\gamma^2/\beta$ . Details are discussed in Sec. III.

With the above definition of the  $p_2$  the collisional Child-Langmuir law becomes

$$\bar{j} = p_2 \varepsilon_0 \sqrt{\frac{2e}{m}} \frac{\bar{V}^{3/2}}{s_m^2} \sqrt{\frac{4\lambda}{\pi s_m}}. \quad (33)$$

The additional square root factor ( $2/\sqrt{\beta}$ ) represents the collisional reduction of the ion flow. Formally, Eq. (33) becomes identical to Eq. (30) for the collisionless case at  $\beta = 4$  or  $\lambda/s_m = \pi/4$ , i.e., at a mean free path of little less than the maximum sheath width, which is quite reasonable. However, one should keep in mind that formula (31) is derived under the assumption of high collisionality, i.e.,  $\beta \gg 1$ , and the transition region of  $\beta \approx 1$  is not necessarily correctly represented.

## F. Collisionless analytical solution

In the collisionless case ( $\beta = 0$ ) only the second derivative remains on the left hand side of Eq. (7). Using again the approximate analytical form for the screening function  $g \approx g_a = \xi^{3/8}$ , the differential equation for  $W$  reads

$$\sqrt{W} W'' = \gamma^2 \xi^{3/8}. \quad (34)$$

An analytical solution to this nonlinear differential equation of the Emden-Fowler type [68] can be found by a simple power ansatz  $W = A\xi^l$ , where  $A$  and  $l$  are constants. Although this ansatz solves the differential equation exactly for  $l = 19/12$  and  $A = \gamma^{4/3} (144/133)^{2/3}$ , it does not fulfil the boundary conditions since it involves  $W(0) = 0$  and  $W'(0) = 0$ . Further, it has no integration constant to adjust. As a rough approximation one can simply add 1 to this solution so that at least the first boundary condition is met and a divergence of the ion density  $n(\xi) = 1/\sqrt{W(\xi)}$  at the sheath edge is avoided. Although then the differential equation is no longer satisfied, the error caused by this approximation is small and differences are noticeable only close to the sheath edge. The approximate solution in the collisionless case is then

$$W(\xi) \approx 1 + \left( \frac{144}{133} \right)^{2/3} \gamma^{4/3} \xi^{19/12}. \quad (35)$$

Adding similarly a term  $\xi\gamma/2$  to the exact solution in order to fulfil also the second boundary condition leads to a strong overestimation of the values for  $W$ . This actually demonstrates also the weak local effect of the second boundary condition

which has a negligible influence on the solution further into the sheath.

With this expression for  $W$  the integrals for calculating the charge and voltage functions  $\tilde{q}$  and  $\tilde{v}$  can be solved:

$$\tilde{q}(\xi) = \xi F\left[\frac{1}{2}, \frac{12}{19}, \frac{31}{19}, -\left(\frac{144}{133}\gamma^2\right)^{2/3} \xi^{19/12}\right], \quad (36)$$

$$\tilde{v}(\xi) = \tilde{q}(\xi) - \frac{\xi^2}{2} F\left[\frac{1}{2}, \frac{24}{19}, \frac{43}{19}, -\left(\frac{144}{133}\gamma^2\right)^{2/3} \xi^{19/12}\right]. \quad (37)$$

Here  $F$  is the hypergeometric function. Although this function and its properties are well tabulated, for practical purposes it is nevertheless desirable to have approximate formulas available based on more elementary functions. Such approximations with excellent accuracy are provided in Appendix D. However, in the discussion of the results presented in Sec. III the above exact forms are used throughout.

It is not possible to derive an explicit analytical expression for the sheath edge position as a function of phase from Eq. (37). Instead, Eq. (36) is inverted approximately. Then  $\xi_s$  is expressed as a function of  $q$  via Eqs. (14) and (36),  $q$  as a function of  $v$  via Eq. (22), and finally  $v$  as function of  $\varphi$  via Eq. (B17). Details of the approximations made in this chain of transformations in order to invert Eq. (36) are given in Appendix D. The approximation made in the second step is the use of the cubic charge-voltage relation. The final result is

$$\xi_s(\varphi) = \left[\frac{(\kappa_1 \{1 - q[v(\varphi)]\} + 1)^{38/5} - 1}{(\kappa_1 + 1)^{38/5} - 1}\right]^{12/19}, \quad (38a)$$

$$\kappa_1 = (2.828\gamma^{4/3} + 1)^{5/38} - 1. \quad (38b)$$

Apparently, the form of the equation ensures exactly the required values at the extremes, i.e.,  $\xi_s(0) = 1$  and  $\xi_s(\pi) = 0$ . It should be noted that the initially more obvious alternative of directly inverting Eq. (37), which would avoid the detour over  $q$ , leads to analytically unsolvable algebraic equations and is not feasible.

### G. Collisional analytical solution

In the collisional case ( $\beta \gg 1$ ) the second derivative  $W''$  in Eq. (7) can be neglected in comparison to the term  $\beta W'$ . Again using the analytical approximation for the screening function  $g \approx g_a = \xi^{3/8}$ , integration becomes straightforward:

$$W(\xi) = (1 + \alpha \xi^{11/8})^{2/3}. \quad (39)$$

In the collisional solution the dependence on the two governing parameters can be expressed by a single parameter  $\alpha = (12/11)\gamma^2/\beta \propto n_0/\lambda$ . With increasing pressure, usually also the plasma density increases while the ion mean free path decreases. Therefore, both effects multiply and a strong increase in the effective parameter  $\alpha$  with pressure can be expected. Naturally, this solution is independent of the second boundary condition.

Like in the collisionless case, the form of  $W(\xi)$  does not allow an exact analytical evaluation of the integrals defining the charge and voltage functions  $\tilde{q}$  and  $\tilde{v}$ . In order to obtain at

least approximate analytical expressions, the same strategy as above is repeated:

$$\tilde{q}(\xi) = \xi F\left(\frac{1}{3}, \frac{8}{11}, \frac{19}{11}, -\alpha \xi^{11/8}\right), \quad (40)$$

$$\tilde{v}(\xi) = \tilde{q}(\xi) - \frac{\xi^2}{2} F\left(\frac{1}{3}, \frac{16}{11}, \frac{27}{11}, -\alpha \xi^{11/8}\right). \quad (41)$$

Similar to the collisionless case, here the sheath edge position can also be calculated approximately as a function of  $q$  (details are given in Appendix D):

$$\xi_s(\varphi) = \left[\frac{(\kappa_2 \{1 - q[v(\varphi)]\} + 1)^{22/13} - 1}{(\kappa_2 + 1)^{22/13} - 1}\right]^{12/11}, \quad (42a)$$

$$\kappa_2 = [1.864\alpha^{2/3} + 1]^{13/22} - 1. \quad (42b)$$

Remarkably, the general structure of the analytical approximations for  $\tilde{q}$  and  $\tilde{v}$  is very similar to the collisionless case, although, the coefficients are different.

The numerical factors in the analytical solutions derived above for the collisionless as well as the collisional case are resulting from the universal exponent of  $\nu = 3/8$  for the single frequency, fully asymmetric discharge. Solutions for arbitrary exponents can be found at the end of Appendix C where also the sensitivity of the solutions to small variations in  $\nu$  is discussed.

While in the collisionless case, the part containing the first derivative vanishes exactly for the limiting case  $\beta = 0$ , in the collisional case, the second derivative would vanish totally only for the unrealistic case  $\beta \rightarrow \infty$ . The two approximations are therefore quite complementary. By neglecting the second derivative in the analytical approximation, the remaining differential equation is solved exactly in the collisional case while in the collisionless case an approximation is necessary to solve an exact differential equation. Finally, the neglect of the second derivatives leads to a dependence of the solution on only one effective parameter  $\alpha$ .

### H. Transition formula

In a systematic approach, the solution for  $W$  can be expanded into an infinite series of functions with terms being proportional to increasing powers of the collision parameter  $\beta$ . Then the sheath differential equation can be expanded and sorted into groups of equations proportional to powers of  $\beta$ . The zeroth order equation represents the fully collisionless case and is naturally identical to Eq. (34) solved above. However, already the first order equation is an inhomogeneous second order differential equation with the equivalent of a ‘‘frequency’’ term that shows a complex spatial dependence. This equation does not have an analytical solution. On the other hand, if numerical integration has to be applied anyway there is no point in not solving directly the full original Eq. (7).

Nevertheless, a more heuristic approach turns out to be successful. The solutions for the extreme cases of collisionality both have the characteristic to diverge in the regions where they do not apply. This motivates a transition formula based on an inverse power scaling:

$$\frac{1}{W^\chi} = \frac{1}{W_1^\chi} + \frac{1}{W_2^\chi}. \quad (43)$$

Here,  $W_1$  and  $W_2$  are the analytical solutions for the collisionless and the collisional cases, respectively. A similar approach is made in [67]. In order to meet the first boundary condition  $W(0) = 1$  by this transition formula, the integration constants for the individual solutions are determined by  $W_{1/2}(0) = (1/2)^{1/\chi}$ . Empirically,  $\chi = 2$  is found to be the optimum value. The transition formula, in fact, applies well for the entire range of collisionality.

### III. DISCUSSION OF THE SOLUTION

In this section the various characteristic sheath quantities are explicitly calculated and the numerical solutions are compared to the analytical approximations. Generally, good agreement between the numerical solutions and the analytical approximations is found for  $\beta \leq 1$  (collisionless case) and  $\beta \geq 10$  (collisional case), respectively. This corresponds to pressures of typically  $p \leq 1$  Pa and  $p \geq 10$  Pa. For the intermediate range the approximate analytical transition formula provides reasonable agreement. In this section, two characteristic collisional parameter cases,  $\beta = 0$  and  $\beta = 6\pi \approx 19$ , are investigated for the same density parameter  $\gamma = 30\sqrt{2} \approx 42$  (Sec. III A). In the collisional case this corresponds to an effective parameter  $\alpha = 104$ . The intermediate range is briefly discussed in Sec. III B. Finally, in Sec. III C the analytical solutions are compared to experimental data from the literature based on laser electric field measurement in the sheath.

Before comparing the various solutions in detail, a further comment, supplementing the discussion in Appendix C, can be made on the second boundary condition and the use of a universal screening function  $g_a$ . By the two analytical solutions derived above an understanding on the insensitivity of the screening function  $g$  to variation of  $\gamma$  and  $\beta$  can be developed easily. Generally, the structure of the differential equation (7) allows removing of  $\gamma^2$  from the equation by applying a transformation  $\tilde{W} = W/\gamma^{4/3}$ . Then the density parameter  $\gamma$  appears in the solution only via the boundary condition  $\tilde{W}(0) = 1/\gamma^{4/3}$ . Apparently, for large values of  $\gamma$  the boundary value of  $\tilde{W}$  goes to zero. This is equivalent to  $W$  rising steeply and becoming effectively independent of the boundary condition. In this case, the dependence on  $\gamma$  is mainly given by a multiplying factor  $\gamma^{4/3}$ , which originates from the differential equation and not from the boundary condition. If now in the integral for the voltage function  $\tilde{v}(\xi)$  the initial value is ignored, this multiplying factor cancels out in the calculation of the normalized sheath voltage  $v$  by the normalizing factor  $\tilde{v}(1)$ . Therefore, only a very weak dependence of  $g$  on  $\gamma$  via the initial value of  $W$  has to be expected. In the highly collisional case the same argument applies to  $\beta$  since it appears only within the effective parameter  $\alpha$  which is also just a multiplying factor within the differential equation. However, in the transition region of small but not yet negligible  $\beta$  a similar argument cannot be developed. However, here the influence of  $\beta$  on the solution is relatively weak and so again there is no significant impact on  $g$ .

#### A. Collisionless and collisional solutions

The screening function  $g(\xi)$ , the normalized drift velocity squared  $W(\xi)$ , and the ion density  $n(\xi)$  are shown in

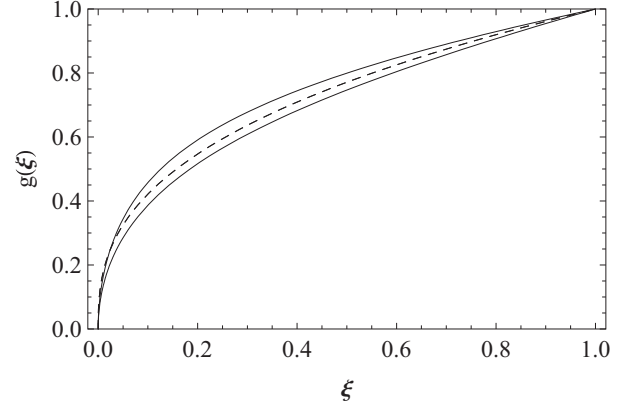


FIG. 4. Screening function: exact numerical solution (solid line), universal analytical approximation (dashed line). The line above the universal analytical approximation represents the collisionless case ( $\beta = 0$ ,  $\gamma = 30\sqrt{2}$ ) and the line below the collisional case ( $\beta = 6\pi$ ,  $\gamma = 30\sqrt{2}$ ).

Figs. 4, 5, and 6, respectively. Very good agreement is found throughout. The drift velocity and the density are especially very well approximated by the analytical solution. In the collisionless case, the increase in  $W$  represents directly the increase in the ion energy. Since ions enter the sheath typically with energies of the order of eV, the value for  $W$  at the electrode of about 150 corresponds to a few hundred eV, which is a typical value for capacitive discharges. From Eq. (36) the scaling of  $W$ , and thereby of the ion energy at the electrode, can be conveniently deduced as  $W(1) \approx 1.05\gamma^{4/3}$ . Correspondingly, the decrease of the ion density towards the electrode scales like  $\gamma^{-2/3}$ . In the present example this yields a density decrease by one order of magnitude. Naturally, in the collisional case the increase of the drift velocity and the decrease of the density is lower. Remarkably, the square of the drift velocity increases almost linearly in the collisional case. This visible behavior can be deduced directly from Eq. (39), which gives a scaling of  $\xi^{11/12}$ , i.e., very close to linear.

In the collisional case, deviations result from the error made by neglecting the second derivative of  $W$  in Eq. (7). The ratio of the second derivative term to the first derivative term is

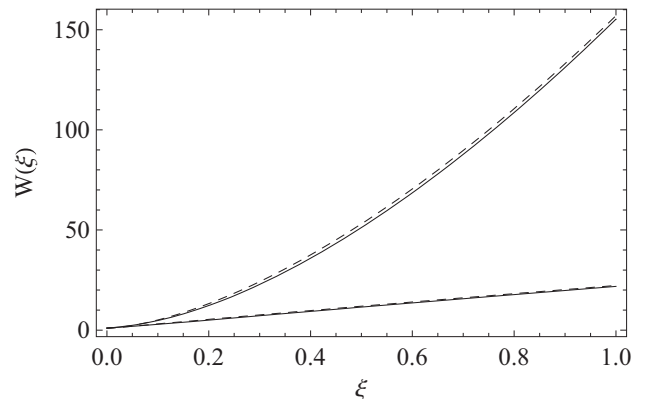


FIG. 5. Square of normalized drift velocity: exact numerical solution (solid line); analytical approximation (dashed line). The upper pair of lines represents the collisionless case ( $\beta = 0$ ,  $\gamma = 30\sqrt{2}$ ) and the lower pair the collisional case ( $\beta = 6\pi$ ,  $\gamma = 30\sqrt{2}$ ).

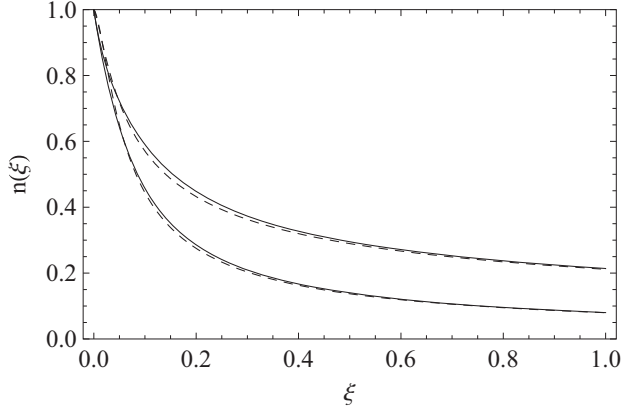


FIG. 6. Ion density: exact numerical solution (solid line); analytical approximation (dashed line). The lower pair of lines represents the collisionless case ( $\beta = 0$ ,  $\gamma = 30\sqrt{2}$ ) and the upper pair the collisional case ( $\beta = 6\pi$ ,  $\gamma = 30\sqrt{2}$ ).

generally negligible. However, very close to the maximum sheath extension where  $W$  has still not increased strongly there is indeed some smaller contribution (Fig. 7). As discussed already in Sec. II B, at maximum sheath extension the right hand side of the differential equation becomes zero so that there the ratio is exactly  $-1$ . From this initial point, the ratio almost immediately crosses zero at about  $\xi_c \approx 0.62\bar{v}(1)(\beta/\gamma)^2 \approx 0.03 \ll 1$  and then exhibits the local extreme discussed above. In summary, the overall behavior supports the approximation made in the analytical solution.

The mean electric field can be calculated in two ways: The natural way would be via integration of the left hand side of Eq. (7), i.e.,  $\bar{F}(\xi) = W'(\xi) - W'(0) + \beta [W(\xi) - W(0)]$ . For the analytical solution this is not without problems since the approximation does not fulfil the boundary condition for the first derivative  $W'(0) = \gamma/2$  and in the collisional case the first derivative is neglected after integration, i.e.,  $\bar{F}(\xi) = \beta [W(\xi) - W(0)]$ . As a consequence, in the collisional case  $\bar{F}$  scales similar to  $W$ , which explains the remarkably close to linear behavior shown in Fig. 8, i.e.,  $\bar{F} \propto \xi^{11/12}$ .

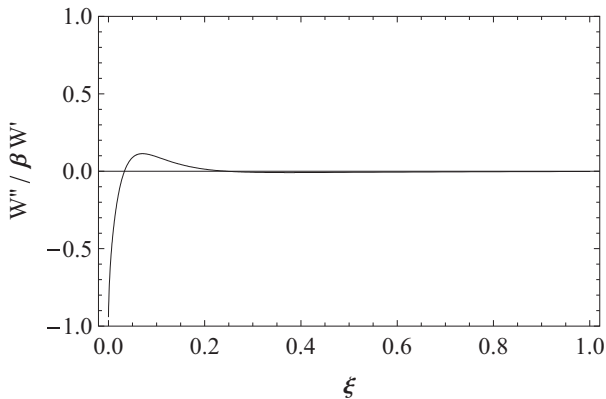


FIG. 7. Ratio of the two terms on the left hand side of the sheath differential equation calculated from the numerical solution for  $\beta = 6\pi$ ,  $\gamma = 30\sqrt{2}$ . The second derivative is contributing slightly only close to the maximum sheath extension.

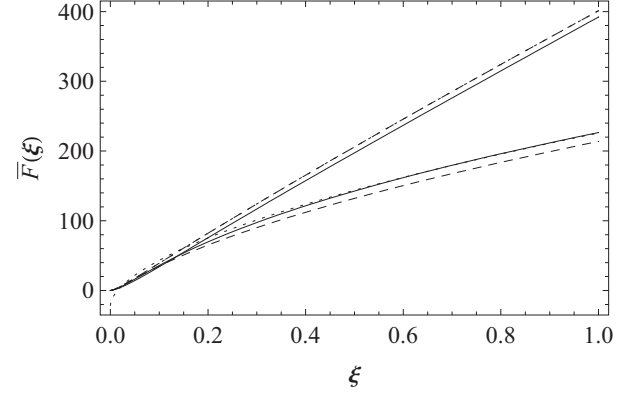


FIG. 8. Mean electric field: exact numerical solution (solid line); analytical approximation based on integration of the left hand side of Eq. (7) (dotted line) and on integration of the right hand side (dashed line). The lower set of lines represents the collisionless case ( $\beta = 0$ ,  $\gamma = 30\sqrt{2}$ ) and the upper set the collisional case ( $\beta = 6\pi$ ,  $\gamma = 30\sqrt{2}$ ). In the collisional case the dashed and dotted lines are effectively on top of each other.

Alternatively, the field can be calculated via integrating the right hand side  $\bar{F}(\xi) = \gamma^2 \int_0^\xi g(\xi')/\sqrt{W(\xi')}d\xi'$ , which avoids the problems at the edge in the collisionless case. Effectively, this means integrating Poisson's equation. Apparently, integration of the left side is closer to the numerical solution in the collisionless case but shows an artificial zero crossing very close to the edge (Fig. 8). This artifact is, in fact, avoided by integration of the right side but differences are more pronounced close to the electrode due to the slight underestimation of the screening function  $g$  in the analytical solution. In the collisional case both alternatives are identical. Generally, the analytical solutions compares very well with the numerical solution which again justifies the approximations made in the derivation.

The cubic correction parameter  $a$  is only weakly dependent on the density parameter  $\gamma$  in the collisionless case (Fig. 9). The exact numerical result based on Eq. (21) is fully

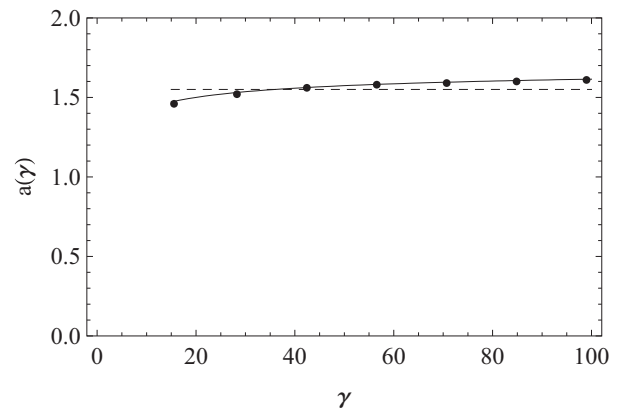


FIG. 9. Cubic correction parameter  $a$  as a function of the density parameter  $\gamma$ : numerical values (dots) and analytical approximation (solid line), both based on Eq. (21). Curves start at the relevant lower limit of  $\gamma \geq 15$ . The dashed line represents a reasonable average value of  $a = 1.55$ .

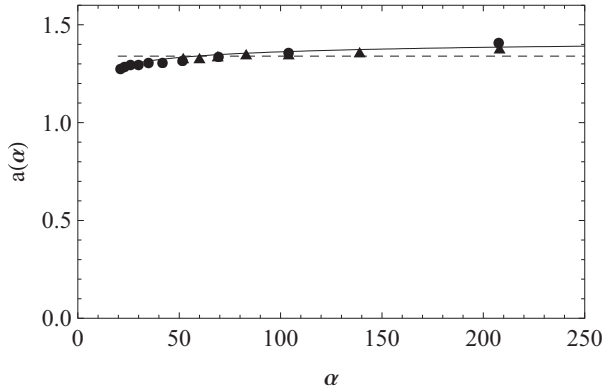


FIG. 10. Cubic correction parameter  $a$  calculated by Eq. (21) as a function of the effective parameter  $\alpha = (12/11)\gamma^2/\beta$ : numerical values for  $\gamma = 42$  (dots) and  $\gamma = 84$  (triangles) and analytical solution (solid line). The dashed line represents a reasonable average case value of  $a = 1.34$ , which is close to the exact value for the parameter case investigated in this section of  $a = 1.36$ . Some of the numerical points for the two different values of  $\gamma$  effectively overlap.

reproduced by the analytical result. Considering that the relevant parameter range starts at  $\gamma \geq 15$ , a constant value applying in good approximation for all  $\gamma$  is about  $a = 1.55$ . This value is also close to the value obtained for the density parameter of  $\gamma = 42$  used in the examples of this section ( $a = 1.56$ ).

In the collisional case, the cubic correction parameter  $a$  should be a weakly dependent function of the effective parameter  $\alpha$ . In Fig. 10 the cubic correction parameter  $a$  is calculated via Eq. (21) for various values of  $\beta$  and two different values of  $\gamma$ , i.e., the  $\gamma$  value used generally in this section and a value larger by a factor 2. For the same  $\alpha$  there is not much difference between the two cases of  $\gamma$  and  $a$  varies only within a very narrow range ( $1.27 \leq a \leq 1.40$ ), when  $\alpha$  is varied over an order of magnitude. Also, here the analytical solution agrees well with the numerical data. Generally, the value of  $a$  is smaller than in the collisionless case and the cubic correction is less pronounced. A general average value is about  $a \approx 1.34$ , which is also close the exact value for the parameter combination investigated ( $\alpha = 104$ ) in this section. The mean value for the collisional case is smaller than for the collisionless case since  $a$  is a measure of the inhomogeneity of the ion density in the sheath, which is more pronounced in the collisionless case.

The charge-voltage relation is shown in Fig. 11. As expected, the relation is not simply quadratic, which would be represented by the diagonal. Excellent agreement is found between the numerical and the analytical solutions where the curves are indistinguishable. Also good agreement is provided by the cubic charge-voltage relation [Eq. (20)] using a cubic correction factor determined from the analytical solution via Eq. (21). In the collisionless case  $a = 1.56$  results and in the collisional case the factor is  $a = 1.36$ . In fact, in the collisional case the cubic form is indistinguishable from both, the numerical as well as the analytical solutions. As discussed above, the cubic correction is less pronounced in the collisional case. This explains also partly the success of the pure quadratic approximation made in the past since this approximation was applied mostly to the collisional case.

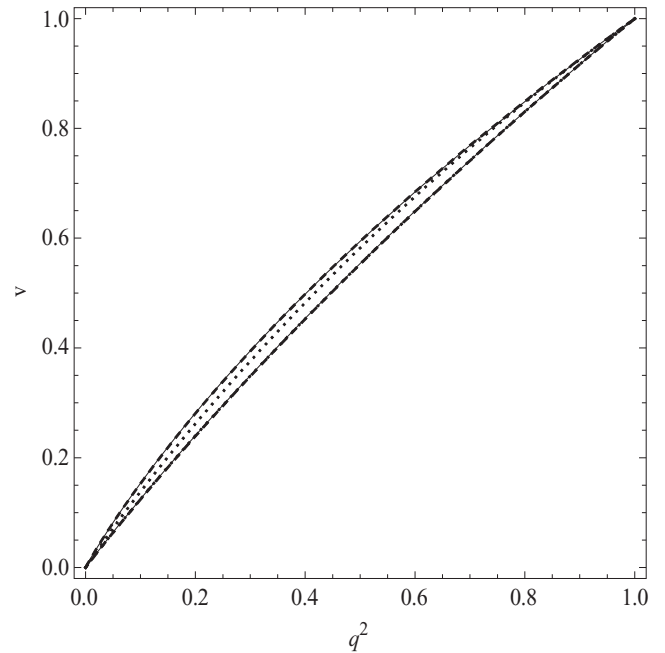


FIG. 11. Charge-voltage relation: numerical solution (solid line); analytical solution (dashed line); and cubic form of the charge-voltage relation from Eq. (20) (dotted line). The upper set of lines belongs to the collisionless case ( $\beta = 0$ ,  $\gamma = 30\sqrt{2}$ , and  $a = 1.56$ ). Here the dashed and the solid lines are effectively on top of each other but the dotted line is slightly off. The lower set of lines belongs to the collisional case ( $\beta = 6\pi$ ,  $\gamma = 30\sqrt{2}$ , and  $a = 1.36$ ): Here all three lines are effectively on top of each other.

The dynamics of the instantaneous sheath edge position  $\xi_s$  is presented in Fig. 12. There is very little difference between the numerical and the analytical solutions. The numerical as well as the analytical solutions are parametric presentations of the form  $\varphi [v(\xi_s)]$ . Further, as explained above with the help of the cubic approximation, an explicit analytical representation also is plotted. Generally, the collisionless case shows lower values of the normalized sheath edge coordinate than the collisional case, i.e., the fractional space-charge region for the same voltage is more extended in the collisionless case. This is a natural result of the lower ion density in sheath for the collisionless case. Further, the figure clearly shows the asymmetry between the extremes. While the dynamic sheath edge spends a rather long time close to the point of maximum sheath extension, it hits the electrode during collapse only for an instance.

Comparison of the dynamic electric field [Eq. (19)] as a function of phase and spatial coordinate shows again very good agreement between the numerical result and the analytical solution for all phases (Fig. 13). The field amplitude is significantly larger in the collisional case, although the value for the density parameter  $\gamma$  is the same. Clearly, collisional friction in the sheath causes higher field amplitudes. Generally, the curvature of the field is smaller than in the collisionless case, which is a consequence of the less rapid decrease of the ion density due to friction. This leads, in particular, to the rather significant difference in the structure of the time averaged field (Fig. 8). The dynamic structure of the fully

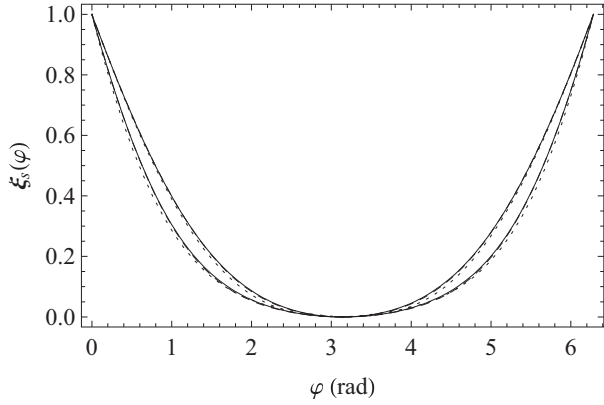


FIG. 12. Dynamics of the instantaneous sheath edge position  $\xi_s$  as function of the rf phase  $\varphi = \omega t$ : numerical result (solid line) and analytical result (dashed line) using both a parametric presentation by  $\varphi [v(\xi)]$ , and explicit analytical approximation (dotted line). The upper set of lines represents the collisional case ( $\beta = 6\pi$ ,  $\gamma = 30\sqrt{2}$ ) and the lower set the collisionless case ( $\beta = 0$ ,  $\gamma = 30\sqrt{2}$ ). For both sets all three lines are effectively on top of each other. It should be noted that for a given phase the same voltage applies in both cases of collisionality.

analytical result is also shown in Fig. 14 for the collisionless case. Clearly the development of the instantaneous sheath edge position can be identified. Further, the temporal variation of the electric field at the electrode is displayed. The result for the collisional case looks quite similar, although the amplitude is higher and the curvature is slightly different, as shown in Fig. 13.

The dynamics of the electric field at the electrode defines also the displacement current density (Fig. 15). The numerical solution and the analytical solution are indistinguishable when using a parametric presentation via Eqs. (25) and (26). The explicit expression based on the approximate determination

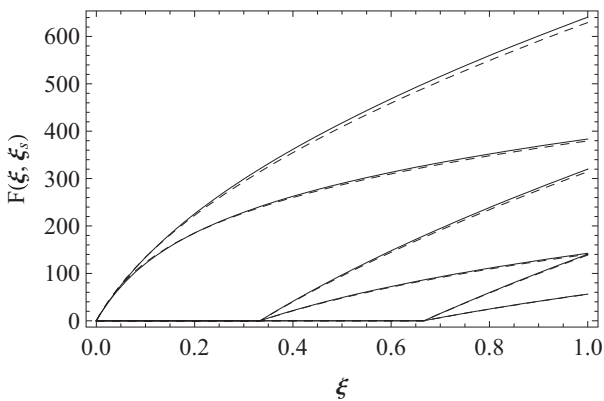


FIG. 13. Dynamic electric field in the sheath as a function of position and for three different rf phases. Here the phase is characterized by the temporary position of the sheath edge which is set to  $\xi_s = 0, 1/3$ , and  $2/3$ : numerical result (solid line); analytical result (dashed line). In all cases the solid and dashed lines are effectively on top of each other. The field is zero for positions  $\xi < \xi_s$ . For a given sheath edge position, the higher field strengths correspond to the collisional case ( $\beta = 6\pi$ ,  $\gamma = 30\sqrt{2}$ ) and the lower field strengths to the collisionless case ( $\beta = 0$ ,  $\gamma = 30\sqrt{2}$ ).

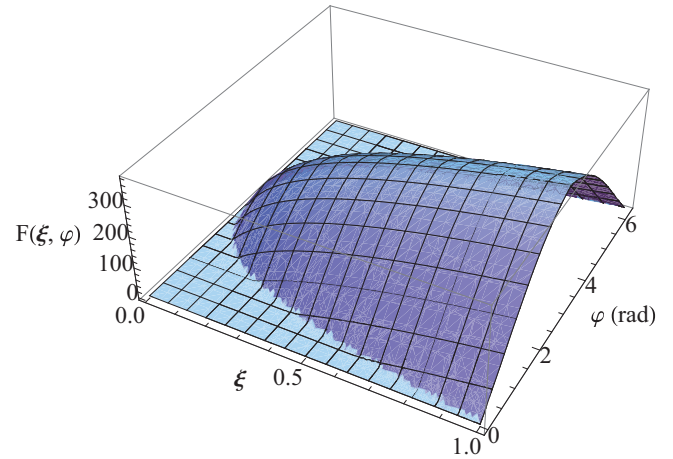


FIG. 14. (Color online) Dynamics of the normalized electric field in the sheath as a function of position and rf phase using the fully analytical result for the collisionless case ( $\beta = 0$ ,  $\gamma = 30\sqrt{2}$ ).

of the sheath edge position as a function of the rf phase slightly underestimates the current at the time of sheath collapse but generally follows very closely the numerical solution. Also the explicit expression based only on the cubic charge-voltage relation is quite close, although deviations are slightly stronger than for the explicit alternative using the sheath edge position. For both explicit expressions, the only input parameter considering the particular sheath properties is the cubic correction parameter  $a$ . However, as shown above, this parameter is effectively a constant ( $a \approx 1.55$ ) not depending on the density parameter  $\gamma$ . Therefore, it can be concluded that the also the current wave form is effectively not depending on the density parameter  $\gamma$ . Comparison is made in Fig. 15 and good agreement is found.

Remarkably, the extremes of the current are not located at the time of the sheath collapse but they appear with a significant phase shift  $\Delta\varphi \approx \pm 1$ . A closer look at Fig. 14 shows that the

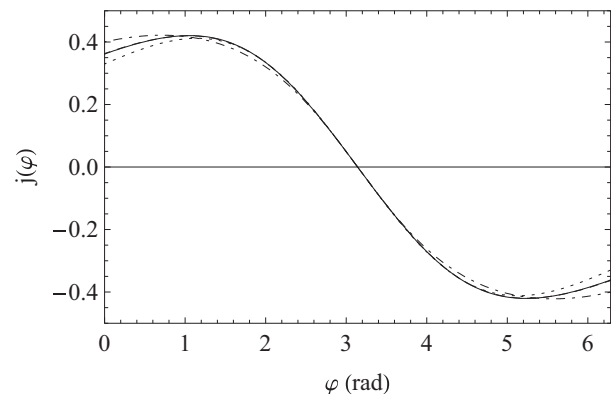


FIG. 15. Normalized displacement current as a function of the rf phase for the collisionless case ( $\beta = 0$ ,  $\gamma = 30\sqrt{2}$ ): numerical solution (solid line); analytical result using a parametric presentation as a function of  $\xi_s$  (dashed line); analytical result using an explicit approximate expression for the sheath edge position (dotted line); and analytical result based only on the cubic charge-voltage relation (dash-dotted line). The solid and the dashed line are effectively on top of each other.

extremes in the temporal slope of the electric field are also not located at the sheath collapse. The shift of the locations for the extremes can be understood by identifying alternatively the current density as the product of the ion density times the sheath edge velocity. For a homogeneous ion density profile, the displacement current would simply be given by the speed of the sheath front and extremes would be located at the collapse (Fig. 12). However, since the density is increasing with distance from the electrode, the current peaks when the sheath is already quite extended ( $\xi_s \approx 0.3$ ). As a consequence, the current density is almost constant over the entire width of the sheath and falls off sharply only close to the point of maximum sheath extension. At the collapse, the sign of the current density changes instantaneously as a consequence of the assumption of total asymmetry. For any finite value of the symmetry parameter ( $\varepsilon > 0$ ), i.e., finite electrode to ground area ratio, the current is zero at the collapse with the slope depending on the symmetry parameter. This is discussed in more detail in Appendix B and in comparison with the experiment. In the collisional case all solutions are effectively indistinguishable. Further, the phase shift effect becomes negligible so that the current is closer to a cosine wave form (with half the rf frequency). Otherwise, shape and amplitude are quite similar so that a separate plot is not shown here.

The coefficient  $p_1(\gamma)$  for the collisionless rf Child-Langmuir law is calculated as function of the density parameter  $\gamma$  in Fig. 16 according to the definitions given by Eq. (29). While both definitions, representing integration of the left and right hand sides of the sheath Eq. (7), give indeed identical values for the numerical solution, the results differ for the approximate analytical solution. When integrating, the universal exponent for the screening function  $g = g_a = \xi^{3/8}$  is used and the integral for the right-hand side solution is carried out numerically. However, the left-hand side yields an explicit expression by the analytical approximation for  $W$  [Eq. (35)]. The figure shows that the latter form is indeed closer to the numerical result. The asymptotic analytical value for large  $\gamma$  is  $p_1 = 133/142 = 0.94$  and the numerical solution is, in

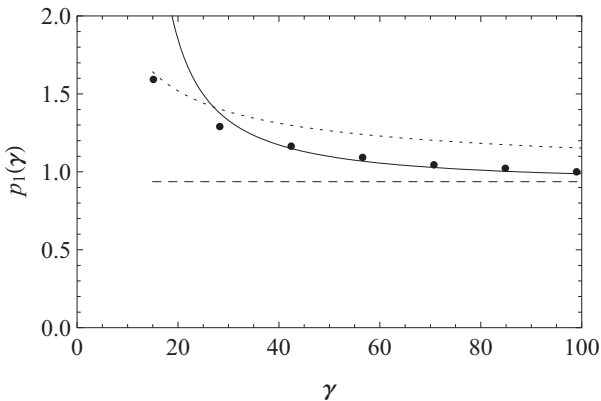


FIG. 16. Coefficient  $p_1(\gamma)$  for the collisionless rf Child-Langmuir law as a function of the density parameter  $\gamma$ : numerical solution (dots); analytical solution using integration of the left hand side (solid line); and right hand side (dotted line) of the sheath equation [Eq. (29)]. The asymptotic value of  $133/142 = 0.94$  is shown by a dashed line. Curves start at the minimum value of  $\gamma = 15$ .

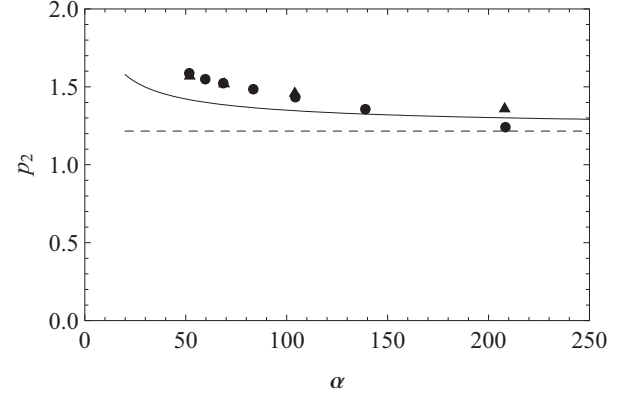


FIG. 17. Coefficient  $p_2$  for the collisional rf Child-Langmuir law as a function of the effective parameter  $\alpha = (12/11)\gamma^2/\beta$ : numerical values for  $\gamma = 42$  (dots) and  $\gamma = 84$  (triangles) and analytical approximation (solid line). The dashed line represents the asymptotic analytical value  $p_2 = 1.22$  for very large  $\alpha$ . Some of the numerical points for the two different values of  $\gamma$  effectively overlap.

fact, converging to this value. Clearly,  $p_1$  is not a constant but varies with  $\gamma$  quite noticeably. An average constant value (within about  $\pm 20\%$ ) for the relevant range of  $\gamma$  can be set at  $p_1 \approx 1.2$ . This value is also very close the exact value for the choice of  $\gamma = 42$  used in this section.

Like in the collisionless case the coefficient  $p_2$  for the collisional rf Child-Langmuir law is not exactly a constant but decreases with the control parameter, in this case  $\alpha$  (Fig. 17). For large values  $p_2$  approaches indeed the asymptotic analytical value. The numerical values calculated for two different values of  $\gamma$  are very close, which demonstrates that the coefficient is indeed only a function of the effective parameter  $\alpha$ . Generally, analytical and numerical values are close.

### B. Intermediate solution

In the intermediate range between the exactly collisionless and the strongly collisional sheath the transition formula [Eq. (43)] can be applied. In Fig. 18 the result is shown for the same density parameter as used above and four different collision parameters in the transition range. Very good agreement is found throughout. Similarly, all derived quantities like, e.g., the density show comparable good agreement between the numerical and the analytical solutions.

### C. Comparison to experimental data

Electric field profiles obtained by laser electric field measurements in rf discharges are available in the literature for various gases and pressures. Spatially and temporally electric fields are obtained by measuring the Stark splitting of Rydberg states of the respective atoms. Here data from our earlier work are used [57,60] that were measured in the so called GEC reference cell [69], which has a small aspect ratio of powered to grounded electrode area so that the discharge is strongly asymmetric, i.e., symmetry parameter  $\varepsilon \ll 1$ . In fact, in all cases the measured sheath voltages can be very well approximated by the square of a sine function as is exactly the case for  $\varepsilon = 0$ , the particular case investigated in this work. Therefore,

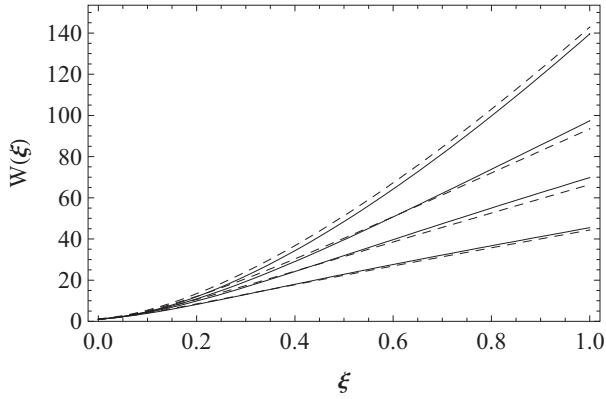


FIG. 18. Square of normalized drift velocity: exact numerical solution (solid line); analytical approximation (dashed line). The different cases are all calculated for the same density parameter  $\gamma = 30\sqrt{2}$  and various values of the collision parameter  $\beta = k\pi$  with  $k = 0.1, 0.5, 1.0, 2.0$  (from top to bottom) representing the transition region between the collisionless and the collisional regime.

the main effect of the finite value of the  $\varepsilon$  is on the displacement current, which is demonstrated later in this section. A more detailed discussion on the effect of discharge symmetry and the definition of the symmetry parameter  $\varepsilon$  can be found in Appendix B. Further details on the experiments and the measurement techniques can be found in the original literature.

Comparison of the analytical solutions of the rf sheath model for  $\varepsilon = 0$  is made with the mean electric field in three different gases (krypton, helium, and hydrogen) under rather different conditions. Temporally averaged field profiles are calculated from the published temporally resolved field profiles. The temporally resolved fields for the collisional case are compared to measurements in krypton and simulations using the Brinkmann sheath model. Actually, hydrogen should be out of the range of applicability of the present model since (a) field reversal appears [59,65,66,70], (b) there is non-negligible ionization within the sheath due to the field reversal, and (c) ions have a complicated collisional dynamics between  $H^+$ ,  $H_2^+$ , and  $H_3^+$  [71]. Nevertheless, the measurement technique in hydrogen is the most precise and sensitive one (minimum field 5 V/cm) and it is instructive to see the comparison for this molecular gas. Helium has a lower sensitivity (minimum field 130 V/cm) but otherwise the precision is similar to that seen with hydrogen. The measurement technique used in krypton has a similar sensitivity (minimum field 100 V/cm) as the one in helium but data are less precise, as can be seen by the rather larger scattering of the data points in Fig. 22. In all figures shown in this section the non-normalized length scale  $x$  is always the distance to the electrode, as indicated in Fig. 1.

In the krypton case at  $p = 1$  Pa the counter electrode in the GEC cell is replaced with a quartz cylinder which further enhances asymmetry so that the self-bias is equal to the rf voltage amplitude, i.e.,  $\varepsilon \approx 0$ . The EEDF is measured by a Langmuir probe close to the sheath edge [60]. The effective electron temperature for the Bohm velocity is inferred from the ensemble average of the inverse energy as defined by the generalized Bohm criterion ( $kT_e^{(\text{eff})} = 2 / \langle 1/\varepsilon \rangle$ ) [72]. This effective value is  $kT_e^{(\text{eff})} = 2.6$  eV, which is close to the effective temperature of the cold part of the EEDF of 2.3 eV.

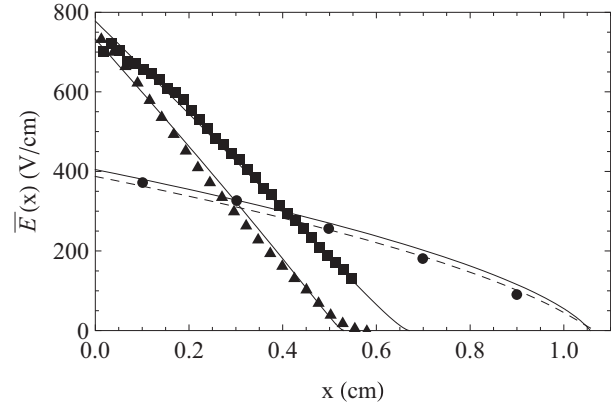


FIG. 19. Mean sheath electric field as a function of the distance from the powered electrode  $x$  for three different cases: krypton at  $p = 1$  Pa (dots), helium at  $p = 50$  Pa (squares), and hydrogen at  $p = 80$  Pa (triangles). The solid lines represent the fields calculated by integrating the left hand side of Eq. (7) using the analytical solutions: helium and hydrogen collisional solution, krypton collisionless solution. In case of krypton, the dashed line represents alternative integration of the right hand side of Eq. (7).

The hot part in the tail of the distribution function has an effective temperature of 7 eV. The corresponding electron density is  $n_0 = 2.0 \times 10^{15} \text{ m}^{-3}$ . Due to the low pressure the sheath is assumed to be collisionless. Further, it is assumed that  $c = 1$ ; i.e., the initial ion velocity equals the classical Bohm velocity. From these data the Debye length and thereby  $\gamma = 57.5$  is calculated. Further, the normalization factor for the electric field follows via  $E_0 = c^2 kT_e / (2s_m)$  to  $E_0 = 1.17$  V/cm. The only free parameter which can be adjusted within a very narrow range is the sheath width  $s_m$ , which is set to  $s_m = 1.07$  cm. In the collisionless case, the mean electric field can be calculated from the analytical solution in two alternative ways, as discussed above in Sec. III A. Both alternatives are very close to each other and compare almost perfectly with the measured data (Fig. 19). Clearly, the mean electric field has a concave shape. It might seem surprising that no information on the sheath voltage is required for the comparison. However, with the initial ion velocity and density being fixed, the sheath voltage follows directly from the sheath width; i.e., the sheath voltage increases with the sheath width. Therefore, the only free parameter here is the maximum sheath width, which is effectively fixed too by the measurement. The same applies to the other cases discussed below.

In case of helium the pressure is much higher and the sheath is clearly collisional. The defining parameters are  $p = 50$  Pa,  $n_0 = 1.9 \times 10^{15} \text{ m}^{-3}$  [57],  $\sigma = 15 \times 10^{-20} \text{ m}^2$  [73], and  $\varepsilon = 0.23$ . The symmetry parameter  $\varepsilon$  is inferred from the measured self-bias and the amplitude of the applied rf voltage via Eq. (B9). In this case, the electron temperature is not known and is chosen as a further fit parameter as  $kT_e = 3.5$  eV, while the maximum sheath extension is set to  $s_m = 0.67$  cm. The parameter  $c$  is again set to  $c = 1$  as it combines with the temperature to one effective parameter. In reality one would expect an initial ion velocity lower than the Bohm velocity so that the temperature would be correspondingly higher. With these parameters  $\gamma = 29.7$ ,  $\beta = 37.9$ ,  $\alpha = 25.4$ ,  $a = 1.30$ , and  $E_0 = 2.61$  V/cm results. Also here the agreement is very

good and in contrast to the collisionless case the field is effectively linear as predicted generally for the collisional case. Very close to the electrode some small deviations might be identified. They can be related either to measurement errors caused by the close vicinity to the electrode surface of less than 1 mm or to some finite dynamics of the light helium ions in the high field region. Nevertheless, the deviations are very small and not really of relevance.

Hydrogen is a special case, as mentioned above. The data from the measurement are  $p = 80$  Pa,  $n_0 = 3.0 \times 10^{15} \text{ m}^{-3}$ , and  $\varepsilon = 0.13$  (inferred from the measured self-bias and the voltage amplitude) [57]. The cross section for charge exchange collisions for  $\text{H}_2^+$  ions is, in fact, rather constant for ion energies above 3 eV at  $\sigma = 10 \times 10^{-20} \text{ m}^2$  [74] and is chosen as the relevant cross section in the model. However, it is clear that this is a substantial simplification since initially only  $\text{H}_3^+$  ions enter the sheath and then a complicated conversion dynamics between the different ion species sets in [58,71]. From a Langmuir probe measurement, the electron temperature is only roughly known as an average value for the entire EEDF of  $\langle kT_e \rangle \approx 2.0$  eV [57]. The value used for the Bohm velocity in the fit is slightly lower at  $kT_e = 1.55$  eV (for  $c = 1$ ) and the maximum sheath width is set to  $s_m = 0.53$  cm. This gives  $\gamma = 44.3$ ,  $\beta = 32.0$ ,  $\alpha = 67.1$ , and  $E_0 = 1.46$  V/cm. The general agreement is again very reasonable and the mean field is effectively linear even in this case. Some systematic deviations might be identified, which are probably real since here the measurement error is certainly the smallest of all three cases. One can even see the smooth transition to zero field strengths at the edge, which is caused by the extended distribution of the electron front due to a finite electron temperature.

The helium measurements are analyzed also with respect to the displacement current density. In the experiment, the displacement current density is inferred from differentiating the measured fields at the electrode surface with respect to time. Comparison with the model using the same input parameters as above shows very good agreement with the data resulting from the differentiated field at the electrode (Fig. 20). For the analytical current density the formula resulting from the cubic charge-voltage relation is used with the analytically calculated cubic correction parameter of  $a = 1.30$  and scaling parameter for the absolute amplitude of  $\tilde{q}(1) = 0.512$ . The results using either Eq. (23) for the fully asymmetric discharge ( $\varepsilon = 0$ ) or the derivative of Eqs. (B14) and (B15) for the experimental symmetry parameter of  $\varepsilon = 0.25$  are compared. Apparently, the latter case is in even better agreement with the experimental points. Remarkably, the small but finite value of the symmetry parameter  $\varepsilon$  removes the artificial discontinuity of the displacement current at the time of the sheath collapse, as discussed in more detail in Appendix B.

The helium data allow also a quite precise determination of the charge-voltage relation. Here a new analysis of the published field and sheath voltage data was performed. By Poisson's equation the positive space charge in the sheath is directly proportional to the electric field at the electrode. The normalized charge  $q$  is then given by the measured electric fields extrapolated to the electrode surface and normalized to the maximum value. The sheath voltage is calculated by the integral over the sheath electric field using an extrapolation

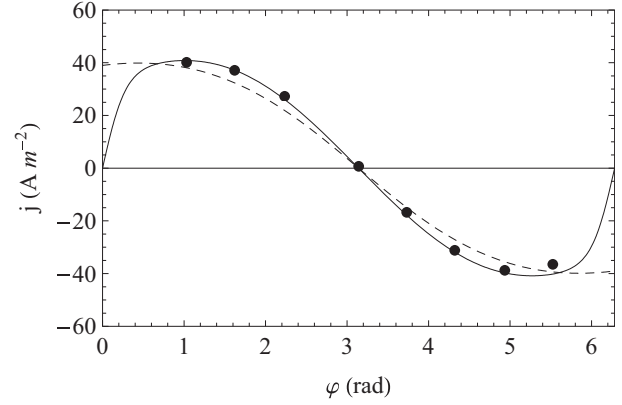


FIG. 20. Absolute displacement current density for the helium discharge at 50 Pa as determined from the experimental data (dots) and the analytical sheath model using the same input parameters as in Fig. 19 in the cubic charge-voltage relation. The cases  $\varepsilon = 0$  (dashed line) and  $\varepsilon = 0.23$  from the experiment (solid line) are compared. The experimental data points are inferred from a direct differentiation of the electric field at the electrode.

to zero at the low-field end. Here again normalization by the maximum value is applied. Naturally, the error in the experimental charge and voltage data is larger for the lower values. The analytical relation uses the same input parameters as listed above (Figs. 19 and 20). Also here experimental data and analytical calculation are in very good agreement (Fig. 21). Clearly, all experimental data are above the diagonal, indicating a cubic correction to the dominant quadratic term. The cubic charge-voltage relation using the calculated cubic correction parameter  $a = 1.30$  is basically indistinguishable

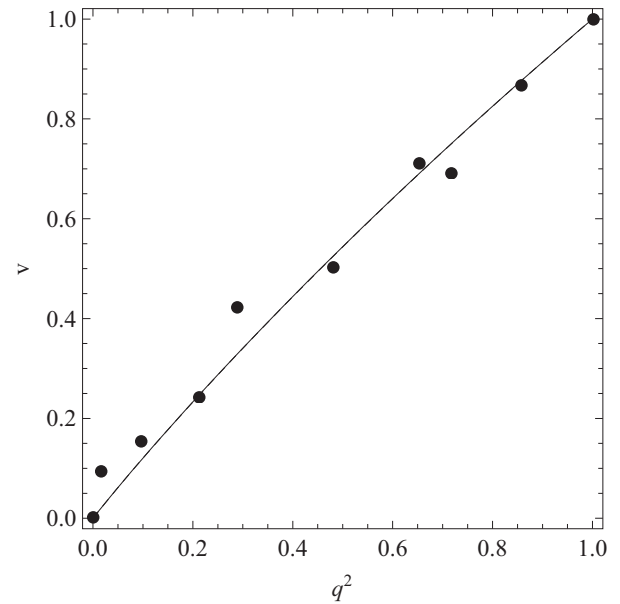


FIG. 21. Charge-voltage characteristic for the helium discharge at  $p = 50$  Pa: dots (measurement); analytically calculated characteristic using the same data as in Figs. 26 and 27 (solid line); cubic charge-voltage relation using the calculated cubic correction parameter  $a = 1.30$  (dashed line). The solid and the dashed lines are effectively on top of each other.

from the analytical solution. The relatively small value explains the moderate deviation from a pure quadratic relation. The high collisionality in this case leads to only a moderate decrease of the ion density towards the electrode surface by only a factor 0.42 [57]. Correspondingly, the cubic correction, which accounts for the inhomogeneity of the ion density in the sheath, is small.

The dynamic electric field is compared in the collisional case of a krypton discharge at  $p = 10$  Pa. As in the 1 Pa case the counter electrode is replaced with a quartz cylinder leading to  $\varepsilon \approx 0$ . From the EEDF measured by a Langmuir probe close to the sheath edge [75] the effective electron temperature for the Bohm velocity is inferred as above from the ensemble average of the inverse energy as defined by the generalized Bohm criterion. This effective value is  $kT_e^{(\text{eff})} = 1.1$  eV, which is only 5% lower than the effective temperature of the cold part of the EEDF. The corresponding electron density is  $n_0 = 7.3 \times 10^{15} \text{ m}^{-3}$ . For comparison, the average electron temperature defined as 2/3 of the mean energy is  $kT_e^{(\text{av})} = 1.9$  eV. Again  $c = 1$  is used due to the lack of knowledge about the exact value. The charge exchange cross section is  $\sigma = 40 \times 10^{-20} \text{ m}^2$  [76]. The maximum sheath width is set to  $s_m = 0.520$  cm. This gives  $\gamma = 82.4$ ,  $\beta = 15.7$ ,  $\alpha = 473$ , and  $E_0 = 1.01$  V/cm, as well as a cubic correction parameter of  $a = 1.41$ . The maximum surface charge density calculated by the model of  $Q = 1.35 \times 10^{-6} \text{ C m}^{-2}$  compares very well with the experimental value of  $Q = 1.3 \times 10^{-6} \text{ C m}^{-2}$ .

Figure 22 shows a comparison of the calculated temporally and spatially resolved field data from the analytical model and the experimental points. Good agreement is obtained throughout considering the measurement errors exhibited by the scattering of the data. Remarkably, the analytical field profiles are effectively identical to the profiles calculated by the Brinkmann sheath model (Fig. 23) [60]. Only at very low field strengths close to the temporary sheath edge do differences

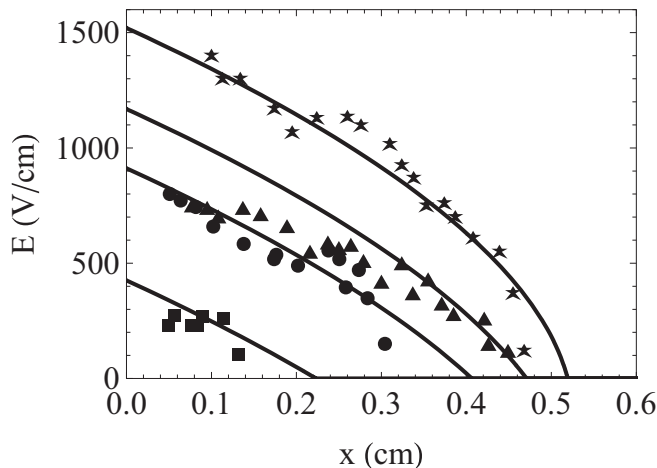


FIG. 22. Comparison of spatially and temporally resolved electric fields in a capacitive rf discharge in krypton at  $p = 10$  Pa. The points are experimental values obtained by laser electric field measurements at different phases of the rf cycle:  $\varphi = 0.639$  (squares),  $\varphi = 1.83$  (triangles),  $\varphi = 3.37$  (stars),  $\varphi = 4.90$  (dots). The aspect ratio and the intervals of the axis are set identical to the original figure taken from Ref. [60], as shown in Fig. 23 for comparison. Here  $x$  is the distance to the electrode.

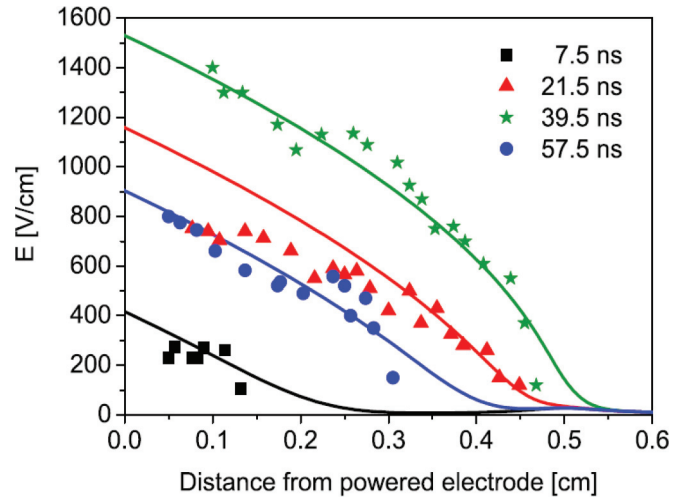


FIG. 23. (Color online) Original figure of the experimental data shown in Fig. 22 and comparison to the computational results using the Brinkmann sheath model [60].

become apparent since the Brinkmann model allows for a smooth transition of the field in the sheath to the ambipolar field in the bulk; i.e., it is not a simple step model but considers the spatial distribution of the electrons around the sheath edge.

It should be noted that the time resolved comparison looks similar for the low-pressure measurements at  $p = 1$  Pa as one would expect already from the time averaged measurement in Fig. 19 and the similarity between the calculated dynamic field structures (Fig. 14). However, due to the one order of magnitude lower krypton atom density, scattering of the measured data points is even stronger [60].

In conclusion, comparison of the fully analytical model to experimental data using *ab initio* plasma parameters, where available, gives excellent agreement for the collisionless as well as the collisional case and time averaged as well as time resolved field profiles are fully reproduced. This strongly supports confidence in the approximations made in deriving the sheath model.

#### IV. SUMMARY AND OUTLOOK

A single second order nonlinear integro-differential equation describing the ion drift velocity in an rf sheath has been derived that depends on two dimensionless parameters. The first parameter is given by the ratio of the maximum sheath extension to the Debye length at this position and is called the density parameter. The second parameter measures the collisionality in the sheath and is proportional to the ratio of the maximum sheath extension to the mean free path for charge exchange.

The model assumes that the wave form of the sheath voltage is known. The sheath voltage is calculated explicitly for the case of a single sinusoidal rf voltage applied to the discharge. Using a cubic charge-voltage relation for both sheaths in a discharge of arbitrary symmetry, the individual sheath voltages are inferred. It is shown that for all relevant cases of different symmetries and cubic contribution to the charge-voltage characteristic, the sheath voltage can be described by some power of a sine function. In this work the particular case of

a fully asymmetric discharge is investigated where the sheath voltage is a sine function squared.

Special attention is paid to the role of the boundary conditions at maximum sheath extension. The step model used for the electron density profile does not allow for an exact derivation of the ion velocity at the boundary. Nevertheless, a reasonable boundary condition ensuring a monotonous and smooth decrease of the ion density is motivated. It is shown that the solution is rather insensitive to this second boundary condition. In particular, the approximate analytical solutions do not depend on this boundary condition but still agree very well with the numerical solution.

Central to the new sheath model presented in this work is the so called screening function describing the screening of the positive ion space charge in the sheath by the temporally averaged electron density. The screening function can be determined self-consistently by solving the sheath differential equation iteratively. It is found that the function has three remarkable properties: First, the final solution is relatively insensitive to small variations of the functional form. As a consequence, the solution converges very rapidly. Second, the self-consistent screening function varies only within close limits for a wide variation of the two characteristic sheath parameters. Third, it is shown that for any parameter combination the screening function can be well approximated by a simple power law with the exponent varying only within a small range. A universal average value for the exponent is proposed which enables approximate analytical solutions to the sheath differential equation. Analytical solutions are found for the collisionless case as well as for the highly collisional case. A simple transition formula combines the two solutions and allows application to arbitrary degrees of collisionality. Very good agreement with self-consistent numerical solutions, experimental data from the literature, and the Brinkmann sheath model is found.

Further, it is shown that the charge-voltage relation can be well approximated by a cubic relation containing a single parameter, the cubic correction parameter. Generally, the cubic contribution is small but more pronounced in the collisionless case. The cubic relation is also used to calculate explicitly the sheath position as a function of the rf phase. This is an important quantity for calculating the dynamic field in the sheath and might be used also in order to calculate the stochastic heating of the electrons. Further, the rf Child-Langmuir laws for the collisionless as well as the collisional case are derived. Both cases are basically identical except for an additional factor that accounts for reduction of the ion current density by collisions in the sheath. In addition, the formulas contain dimensionless factors which depend weakly on the sheath parameters.

Naturally, the model should be compared to PIC/MC simulations. In typical one-dimensional codes the discharge is symmetric ( $\varepsilon = 1$ ), in contrast to the case studied in this work where a fully asymmetric ( $\varepsilon = 0$ ) discharge is investigated. Sheath voltages, plasma parameters, and boundary conditions can be taken directly from the simulation in order to calculate the dimensionless parameters for the model. The exponent for the sheath voltage will then be different and accordingly also a different screening function will be found. For instance, with a typical cubic correction parameter of  $a = 1.5$ , the exponent for

the sine wave form of the sheath voltage is  $k = 3.3$ . The model might also be extended to nonsinusoidal rf voltages, as is, e.g., the case in connection with the electrical asymmetry effect [41,61–63] or for Gaussian wave packages. First investigations in these directions already look very promising. Again, first the individual sheath voltages are approximated in a very similar way on the basis of the cubic charge-voltage relation. Second, an analytical approximation for the screening function is found. However, this is still work in progress that will be the subject of future publications.

Although already a great number of sheath quantities has been calculated already in this work there are still some important quantities missing. On the basis of the calculated temporally and spatially resolved electric fields, ion energy distribution functions at the electrode could be inferred using, e.g., the Monte Carlo technique first applied by Wild and Koidl [17]. Investigations into stochastic electron heating are another challenge. Here the calculated sheath edge velocity and ion density profile could be combined with analytical models presented recently in the literature [53–56].

In conclusion, the analytical sheath model allows convenient calculation of all relevant sheath properties. Comparison with experimental data shows excellent agreement and confirms the viability of the underlying assumptions. Nevertheless, detailed comparison with PIC simulations is desirable. Extension of the model to symmetric discharges, multifrequency discharges, determination of ion energy distribution functions, and stochastic electron heating should be straightforward.

## ACKNOWLEDGMENTS

This work was stimulated by a sabbatical stay at the University of Texas at Dallas and an invited talk at the University of Wisconsin at Madison. The author is very much indebted to Matthew Goeckner and Chun Lin for their support. Further, fruitful discussions with Edmund Schüngel, Julian Schulze, Tsanko Tsankov, Zoltan Donko, Ralf Peter Brinkmann, and Thomas Mussenbrock are gratefully acknowledged.

## APPENDIX A: DERIVATION OF THE SIMPLIFIED MOMENTUM BALANCE EQUATION

The calculation starts with the stationary Boltzmann equation but then the moments are built in order to derive the fluid equations. The use of the stationary equation including only the time averaged functions for the ion distribution and the electric field is justified for sufficiently high rf frequencies and high ion inertia. For the particular case of a spatially linearly varying field an exact solution to the stationary Boltzmann equation was found by Lawler [77] in connection with analyzing a dc discharge. As shown in this paper, the temporally averaged electric field in the sheath is, in fact, close to linear in the collisional case and deviations are still reasonably moderate in case of the collisionless sheath. Therefore, this linear field solution is of particular importance for the investigation of the rf sheath and can be used to estimate the error made in the approximate form of the momentum balance equation. The stationary Boltzmann equation for the ion velocity distribution function  $f(v)$  with the Wannier collision operator [78] for

charge exchange collisions with a constant mean free path  $\lambda$  is

$$v \frac{\partial f}{\partial x} + \frac{eE(x)}{m_i} \frac{\partial f}{\partial v} = -\frac{|v|}{\lambda} f + \delta(v) \int_{-\infty}^{\infty} \frac{|v|}{\lambda} f dv, \quad (\text{A1})$$

where  $m_i$  is the ion mass,  $e$  the charge of the ion,  $v$  the ion velocity,  $x$  the spatial coordinate, and  $E$  the electric field.

The zero moment of the Boltzmann equation gives the continuity equation  $\partial(nu)/\partial x = 0$ , with  $n$  representing the ion density. The first moment can be arranged as a first order differential equation for  $W = u^2/u_0^2$ , with  $u = \langle v \rangle$ .  $W$  is the normalized square of ion drift velocity and  $u_0$  represents the drift velocity by which ions enter the sheath at its maximum temporal extension  $s_m$ . Using normalized coordinates and variables as introduced in Sec. II A and Fig. 1, the momentum conservation equation can be expressed in a compact form:

$$h_1(\xi) \frac{\partial W}{\partial \xi} + h_2(\xi) \beta W = F(\xi). \quad (\text{A2})$$

Here  $\xi$  is the normalized spatial coordinate and  $F$  is the normalized electric field. The two functions  $h_1$  and  $h_2$  are defined as follows:

$$h_1(\xi) = \frac{\langle v^2 \rangle}{u^2} = 1 + \frac{T_i}{W} \quad \text{and} \quad h_2(\xi) = \frac{2}{\pi} \left( h_1 + \frac{\pi}{\beta} \frac{\partial h_1}{\partial \xi} \right). \quad (\text{A3})$$

Here a normalized (normalization by  $m_i u_0^2/k$ ) one-dimensional local ion temperature  $T_i = \langle v^2 \rangle/u_0^2 - W$  has been defined. Both  $T_i$  and  $W$  are functions of the spatial coordinate  $\xi$ . At this point it is tempting to set the ion temperature or at least the gradient simply to zero as is often done when dealing with ions in low temperature plasmas. However, this is not the approximation proposed in this work. As shown below, at high collisionality the thermal energy contributes about 1/3 to the total energy. The development of the ion temperature is defined by the second moment of the Boltzmann equation. However, adding another equation to the already complicated system would strongly enhance complexity. Further, in order to have explicit expressions for the transport coefficients, the distribution function needs to be known. Assuming simply a shifted Maxwell distribution for the ion velocity distribution would be an approximation in itself with a doubtful accuracy in this case.

For the particular case of a linearly varying field  $E = E_0 \xi$  and assuming a finite ion flux density  $j$  but zero velocity at the sheath edge, the Boltzmann equation has an exact solution, which was derived by Lawler [77]:

$$f(w, \zeta) = f_0 e^{-\zeta} \left\{ \delta(\zeta^2 - w) \theta(w) + \frac{1}{2} [\theta(w) - \theta(w - \zeta^2)] \frac{e^{\sqrt{\zeta^2 - w}}}{\sqrt{\zeta^2 - w}} \right\}. \quad (\text{A4})$$

Here the new variables  $\zeta = \beta \xi/\pi$ ,  $w = mv^2 s_m/(eE_0 \lambda^2)$ , and  $f_0 = 2jms_m/(eE_0 \lambda^2)$  are introduced in order to give the solution a more compact form. From this kinetic solution the exact form of the squared drift velocity  $W$  can be calculated.

$$\beta \sqrt{W} = \frac{\pi \zeta e^{\zeta}}{1 + \frac{\pi}{2} \zeta [I_0(\zeta) + L_0(\zeta)]}, \quad (\text{A5})$$

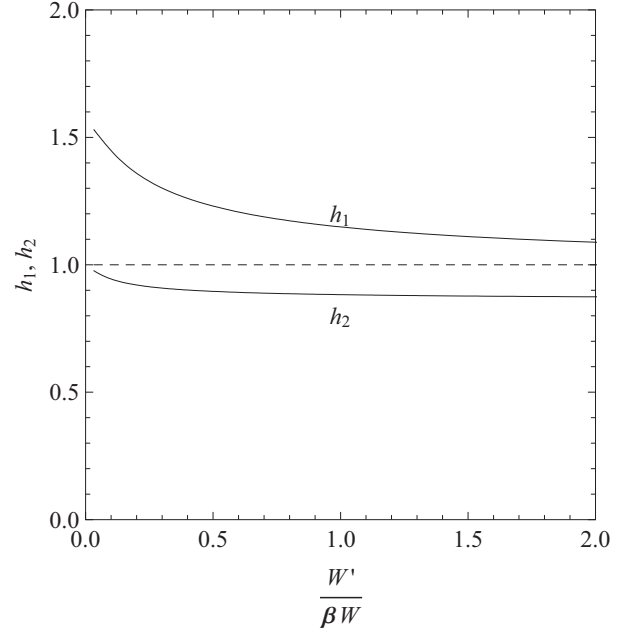


FIG. 24. The function  $h_1$  (upper solid curve) and  $h_2$  (lower solid curve) for a linear electric field as a function of  $W'/\beta W$ . The dashed line is at 1 to indicate the value used in the fluid equation.

where  $I_0$  and  $L_0$  are the modified Bessel function of first kind and the modified Struve function, respectively. Further, the exact form of the functions  $h_1$  and  $h_2$  (via  $h_1$ ) is now also defined:

$$h_1 = \frac{\pi}{2} e^{-2\zeta} [I_1(\zeta) + L_{-1}(\zeta)] \left\{ 1 + \frac{\pi}{2} \zeta [I_0(\zeta) + L_0(\zeta)] \right\}. \quad (\text{A6})$$

It is important to note that  $h_1$  and  $h_2$  depend only on  $\zeta = \beta \xi/\pi$  and not on any other parameter. This effective length scales linearly with the collision parameter  $\beta$ , i.e., at high collisionality the same result is found as at low collisionality but on a shorter real length scale. The solution shows that  $W$  quickly becomes a linear function of the spatial coordinate which indicates the usual drift behavior  $u \propto \sqrt{E}$ . However, it is actually more interesting to study the dependence on  $W'/\beta W$ , where the stroke indicates the derivative with respect to  $\xi$ . Figure 24 shows that when the derivative part has little influence ( $W'/\beta W \ll 1$ ) the function  $h_2$  is close to 1. On the other hand, when the derivative dominates the behavior of the fluid equation ( $W'/\beta W \gg 1$ ), function  $h_1$  is close to 1. In the limit of high collisionality apparently  $h_1 \rightarrow \pi/2$  and the ratio of thermal energy to total energy becomes  $1 - 2/\pi \approx 0.36$ . Clearly, this contribution cannot be ignored and simply setting  $T_i$  to zero in Eq. (A2) is not a valid approximation. In conclusion, this motivates the replacement of both functions by simply a factor 1 in Eq. (1). The equation becomes exact at the two extremes  $\lim \beta \rightarrow 0$  and  $\lim \beta \rightarrow \infty$ .

The solution of the simplified fluid equation (1) for the same linear field is

$$\beta \sqrt{W} = \sqrt{\pi \zeta - 1 + e^{-\pi \zeta}}. \quad (\text{A7})$$

For large values of  $\zeta$ , the solution converges to  $\beta \sqrt{W} = \sqrt{\pi \zeta}$ . Using the normalizing field defined above  $E_0 = mu_0^2/(2es_m)$

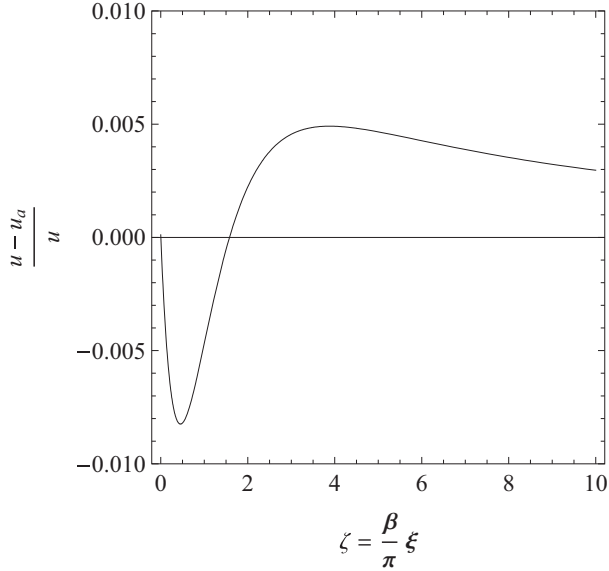


FIG. 25. Error in the drift velocity by use of the simplified fluid equation for a linear electric field ( $u$ , exact solution;  $u_a$ , solution of the simplified fluid equation) as function of the spatial coordinate.

(see Sec. II A), this is equivalent to  $u = \sqrt{2\lambda e E / (\pi m)}$ , i.e., the well known result for the ion drift velocity in a homogeneous field [1,78]. Comparison with the exact kinetic solution shows that the deviation in the drift velocity  $u \propto \sqrt{W}$  is actually smaller than 0.83% throughout (Fig. 25). This finally justifies the simplifying assumptions made for the momentum balance equation. As is shown in Sec. II, the mean electric field found in the rf sheath is actually close to linear, which further supports justification of the approximations made here.

## APPENDIX B: CHARGE-VOLTAGE RELATION AND SHEATH VOLTAGE WAVE FORM

The sheath model is based on the assumption that the time dependent sheath voltage wave form is known. However, in praxis only the applied rf voltage wave form coming from the generator is known and the self-bias and the sheath voltage wave forms have to be determined by a model. The applied rf voltage must be balanced by the sum of the voltages over the sheaths at the powered electrode and ground and the voltage drop over the bulk. In many cases the bulk voltage can be neglected in comparison to the sheath voltages. Important exceptions are discharges at high pressures (typically  $p \gg 100$  Pa), highly electronegative discharges, or the excitation of plasma series resonance oscillations in low-pressure, highly asymmetric discharges [59,60,62,63,79]. The sheath voltages can be determined by using the voltage balance if they are expressed by the positive space charge in the sheath [62]:

$$v(q) = \sum_{j=0}^{\infty} \alpha_j q^j. \quad (\text{B1})$$

Here  $v$  is the sheath voltage and  $q$  the positive space charge in the sheath. Both quantities are assumed to be normalized to their maximum values. Further, conservation of the total space charge in both sheaths is assumed; i.e.,  $q_g = 1 - q$  if  $q$  is the

space charge at the powered electrode and  $q_g$  the space charge at the grounded electrode [61,62].

This concept has been applied successfully to the description of capacitive rf discharges, in particular to the electrical asymmetry effect and the plasma series resonance [59,61,62]. There the charge-voltage relation in the sheath was assumed to show a simple quadratic dependence. A detailed discussion of this approach was made in connection with the so called electrical asymmetry effect [61]. The quadratic relation would apply exactly for a homogeneous ion density. Since the ion density is generally decreasing towards the electrode, in reality also higher order terms of the space charge contribute and deviations become obvious in comparison to simulation results [41,61,63]. Here the problem is revisited and it is shown that generally a cubic approximation is sufficient to describe the charge-voltage relation with high precision. Further, the cubic form will be used to calculate the sheath voltage in discharges of various symmetries.

The charge-voltage relation can contain no constant term since the sheath voltage vanishes at zero space charge, i.e., at the sheath collapse:  $v(q=0) = 0$ . From the first derivative of  $v$  with respect to  $q$  it follows that also the linear term does not exist:

$$\frac{\partial v}{\partial q} = \left( \frac{\partial q}{\partial \xi_s} \right)^{-1} \frac{\partial v}{\partial \xi_s}. \quad (\text{B2})$$

The partial derivatives can be evaluated by Eqs. (14) to (17):

$$\frac{\partial v}{\partial q} = \frac{\tilde{q}(1)}{\tilde{v}(1)} (1 - \xi_s). \quad (\text{B3})$$

Since the space charge vanishes only when the sheath collapses ( $\xi_s = 1$ ), i.e.,  $q(1) = 0$ , it follows that no linear term exists:

$$\left. \frac{\partial v}{\partial q} \right|_{q=0} = \left. \frac{\partial v}{\partial q} \right|_{\xi_s=0} = 0. \quad (\text{B4})$$

Now normalization demands that  $v(q=0) = 0$  and  $v(q=1) = 1$ . Then a cubic ansatz must have the following form:

$$v(q) = q^2 + (a-1)q^2(1-q). \quad (\text{B5})$$

Here  $a \geq 1$  is the cubic correction parameter. For  $a = 1$  the relation would be simply quadratic. Apparently the cubic correction vanishes at  $q = 0$  and  $q = 1$ . The cubic correction parameter can be determined from a known relation  $v(q)$ , e.g., from simulation, by a least mean square fit [similar to Eq. (C1)]. Straightforward calculation yields

$$a = 105 \int_0^1 q^2(1-q)v(q) dq - 2.5. \quad (\text{B6})$$

The integral can, in principle, be carried out numerically. However, in case of the numerical solution for  $W$ , transformation from  $q$  to  $\xi$  is required and in case of the analytical solutions an explicit expression can be found only using again the cubic approximation. Therefore, an alternative procedure is proposed here that avoids these problems.

The first derivative of Eq. (B5) with respect to  $q$  must be equal to Eq. (B3). By making use of the fact that  $\xi = 0$

corresponds to  $q = 1$ ,  $a$  follows as

$$a = 3 - \frac{\tilde{q}(1)}{\bar{v}(1)}. \quad (\text{B7})$$

This fit of the slope is actually carried out at the point of steepest decent of the ion density, i.e., where deviations from a homogeneous density are most pronounced. Once a solution  $W(\xi)$  has been found, the cubic correction can be calculated directly. Generally, the value of  $a$  depends on the two control parameters  $\beta$  and  $\gamma$ .

Now the two sheaths in the discharge can be combined in a voltage balance. Neglecting the bulk voltage and using space-charge conservation to connect the charges in the two sheaths, the following equation results:

$$\eta + v_{rf} = \phi[-q^2 - (a-1)q^2(1-q) + \varepsilon(1-q)^2 + \varepsilon(b-1)(1-q)^2q]. \quad (\text{B8})$$

Here  $\eta$  is the self-bias,  $v_{rf} = v_{rf}(\varphi)$  the rf voltage applied to the discharge with  $\varphi = \omega t$ ,  $\phi$  the voltage amplitude at the powered sheath, and  $\varepsilon$  the ratio of the amplitudes of the two sheath voltages, the so called symmetry parameter.  $a$  and  $b$  are the cubic correction parameters for the two sheaths. The self-bias and the amplitude are related to the extremes of the applied voltage wave form  $\max(v_{rf}) = v_+$  and  $\min(v_{rf}) = v_-$ , respectively:  $q(v_{rf} = v_+) = 0$  and  $q(v_{rf} = v_-) = 0$ . This leads to

$$\phi = \frac{v_+ - v_-}{1 + \varepsilon} \quad \text{and} \quad \eta = -\frac{v_+ + \varepsilon v_-}{1 + \varepsilon}. \quad (\text{B9})$$

The above expressions for the amplitude ratio and the self-bias are identical to those derived earlier [61,62]. The simple reason is that the derivation requires only the general properties of the normalized sheath voltages  $v(q=0) = 0$  and  $v(q=1) = 1$  and conservation of the total space charge. It does not depend on the particular form of the charge-voltage relation. As an important consequence, the so called electrical asymmetry effect, i.e., the formation of a self-bias by an applied voltage wave form with different positive and negative amplitudes, is independent of the cubic or any higher contribution to the charge-voltage characteristic [61].

Experimentally, the symmetry parameter  $\varepsilon$  can be determined from a simple measurement of the bias and the peak voltages via Eq. (B9). The general relation between the symmetry parameter and sheath properties is derived in Refs. [61,62]:

$$\varepsilon = \frac{I_{sg} \bar{n}_{sp}}{I_{sp} \bar{n}_{sg}} \left( \frac{A_p}{A_g} \right)^2. \quad (\text{B10})$$

Here  $I_s$  denotes the sheath integral for the sheaths at the powered and grounded electrodes (indicated above by the indices  $p$  and  $g$ ) and  $\bar{n}_s$  the corresponding spatial mean ion density in the sheath. In the notation of this work the mean ion density is obviously  $\bar{n}_s = n_0 \tilde{q}(1)$  and the sheath integral reads

$$I_s = 2 \frac{\bar{v}(1)}{\tilde{q}(1)} = \frac{2}{3-a}. \quad (\text{B11})$$

The link to the cubic correction parameter is given by Eq. (B7). In Ref. [61] it is shown that the sheath integral can only vary between 1 (flat density profile) and 2 (infinitely steep profile). This limits the possible range for  $a$  to  $1 \leq a \leq 2$ , although at

the upper limit higher order contributions in  $q$  could become important. For a homogeneous ion density in the sheath, a pure quadratic relation applies ( $a = 1$ ) and the sheath integral is indeed 1. This allows also interpretation of  $a$  as a measure of the inhomogeneity of the ion density in the sheath. A more typical value is  $a = 1.5$ , which gives a value for the sheath integral of  $I_s = 1.3$ . The relative variation range of the sheath integral around this value is identical to the range where  $a$  varies. The realistic range is generally smaller than the ultimate limits and will typically be within  $\pm 17\%$ . Apparently, the sheath integral is indeed rather insensitive to variations in the ion density profile and the ratio of the two sheath integrals in the definition of the symmetry parameter will be close to unity for most cases as predicted in Ref. [61].

Although in general the cubic corrections for the two sheaths can be different, it is assumed in the following that they are identical. The cubic corrections depend mainly on the collisionality. Therefore, if the voltages over the two sheaths are not strongly different, i.e., if the discharge is not too asymmetric, the two parameters will be very close. On the other hand, in a strongly asymmetric discharge ( $\varepsilon \approx 0$ ), the sheath voltage at ground becomes negligible. However, neglecting the bulk voltage in the fully asymmetric and collisionless case is not entirely correct since here the inertia of the bulk electrons, represented by a term proportional to  $\tilde{q}$ , together with the nonlinear charge-voltage characteristic of the sheath can lead to strong high frequency oscillations of the displacement current. These so called self-excited plasma series resonance (PSR) oscillations, with typically an order of magnitude higher frequency than the applied radio frequency, involve also small oscillations of the sheath voltage [59]. However, these oscillations cannot affect the ion motion and are not of interest in the context of this paper.

Under these assumptions the voltage balance equation can be rearranged using the abbreviation  $r = (\eta + v_{rf})/\phi$ :

$$r = -q^2 + \varepsilon(1-q)^2 + (a-1)q(1-q)[\varepsilon - q(1+\varepsilon)]. \quad (\text{B13})$$

This cubic equation can be solved exactly. However, since the cubic correction can be expected to be small, a first order perturbative solution in  $(a-1)$  is easier to handle and still sufficiently accurate even at the upper limit of  $a = 2$ :  $q \approx q_0 + (a-1)q_1$ , where  $q_0$  is the solution obtained for the pure quadratic case ( $a = 1$ ):

$$q_0 = \frac{-\varepsilon + \sqrt{\varepsilon - (1-\varepsilon)r}}{1-\varepsilon}, \quad (\text{B14})$$

$$q_1 = \frac{q_0(1-q_0)[\varepsilon - q_0(1+\varepsilon)]}{2[q_0(1-\varepsilon) + \varepsilon]}. \quad (\text{B15})$$

Keeping the solution at first order, the voltage over the sheath at the powered electrode becomes

$$v_s = -\phi \{ q_0^2 + (a-1)[2q_0q_1 + q_0^2(1-q_0)] \}. \quad (\text{B16})$$

There is no significant difference between this explicit first order perturbative solution and the exact parametric solution of the sheath voltage [for a single radio frequency:  $\varphi(q) = \arccos[v_{rf}(q)]$  and  $v_s = -\phi v(q)$ , with  $0 \leq q \leq 1$  and use of Eqs. (B5) and (B13)] for the entire range of possible values for  $\varepsilon$  and  $a$ . Remarkably, for  $\varepsilon = 0$  (totally asymmetric discharge)

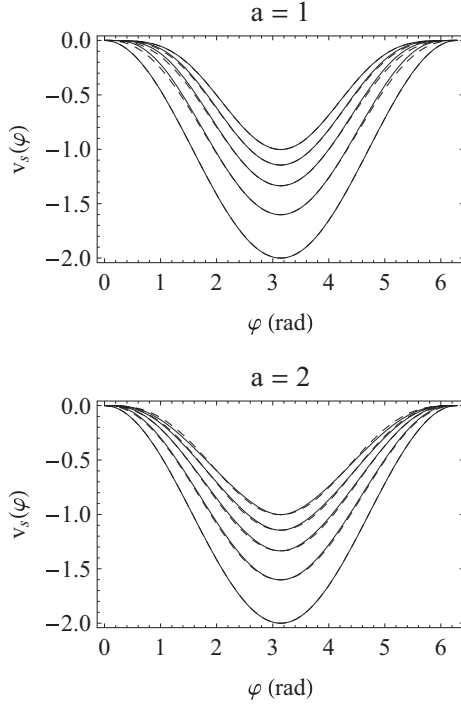


FIG. 26. Voltage wave form over the sheath at the powered electrode in case of  $a = 1$  (top figure) and  $a = 2$  (bottom figure) for various values of the symmetry parameter  $\varepsilon$  (top to bottom):  $\varepsilon = 1, 0.75, 0.5, 0.25, 0$ . The solid lines represent the exact form given Eq. (B16) and the dashed lines the approximation given by Eq. (B17).

the above solution becomes simply  $v_s = -\phi v = -\phi q_0^2 = v_{rf} - v_+ \leq 0$ . This result had to be expected naturally already from the beginning but it is a nice test of consistency here. Therefore, in the totally asymmetric discharge there is no cubic correction to the sheath voltage. In case of a single radio frequency  $v_{rf} = \cos(\varphi)$ , the sheath voltage at the powered electrode becomes simply  $v_s = -2\sin^2(\varphi/2)$ . This is the result used in the present paper. For clarity, it should be noted that by definition  $v_s$  is negative and varies between  $-\phi$  and 0, while  $v$  is positive and varies between 0 and 1.

A closer inspection for a single frequency discharge shows that both the symmetry parameter  $\varepsilon$  and the cubic correction parameter  $a$  can have a significant influence on the wave form. Nevertheless, a reasonably precise empirical approximation to the more complicate exact form can be found, as is demonstrated in Fig. 26:

$$v_s \approx -\phi[\sin^2(\varphi/2)]^{(1+\varepsilon/a)}. \quad (\text{B17})$$

In the above representation the square is explicitly separated from the factor  $(1 + \varepsilon/a)$  since this avoids any ambiguities possibly caused by the alternating sign of the sine function. The amplitude  $\phi$  is defined by Eq. (B10). This simplified form for the wave form is the motivation for using a simple power factor  $k$  for the sheath voltage in Sec. II A. Here, this factor is identified as  $k = 2(1 + \varepsilon/a)$ . Equation (B17) reproduces the exact solutions for the fully asymmetric case  $\varepsilon = 0$  with arbitrary  $a$  ( $k = 2$ ) as well as the symmetric case  $\varepsilon = 1$  with a pure quadratic relation  $a = 1$  ( $k = 4$ ). The power for the symmetric case changes for a strong cubic correction of  $a = 2$

to  $k = 3$  so that there generally the exponent is in the range  $3 < k < 4$ . The negative sign of the sheath voltage at the powered electrode results from the definition of ground at the opposite electrode. In the main part of the paper, where only a single sheath in a fully asymmetric discharge is considered, the sign is taken as positive as this is more convenient.

Both parameters,  $\varepsilon$  and  $a$ , have a strong impact on the current wave form. If the cubic correction is negligible, the current wave form in the fully asymmetric case ( $\varepsilon = 0$ ) is a cosine function at half the radio frequency with a discontinuous change of sign at the instant of sheath collapse at the powered electrode, while it is a sine function at the radio frequency in the symmetric case ( $\varepsilon = 1$ ). The cubic correction is generally adding higher harmonic components to the current. Naturally, in all cases the current has to pass zero twice within an rf period, corresponding to the times of collapse of the two sheaths:  $q(\varphi = 0, \pi) = 0, 1$ . The slope of the normalized current density at these zero crossings [ $\dot{q}(\varphi = 0, \pi)$ ] can be obtained easily for arbitrary values of the symmetry parameter:  $(1 + a)(1 + \varepsilon)/(8\varepsilon)$  at  $\varphi = 0$  (collapse of the sheath at the powered electrode) and  $-(1 + a)(1 + \varepsilon)/8$  at  $\varphi = \pi$  (collapse of the sheath at the grounded electrode). Therefore, the first slope becomes infinite only for  $\varepsilon = 0$ , i.e., for an infinitely large grounded area where the second sheath vanishes. Experimentally, the area ratio and the symmetry parameter are always finite and a steep but finite slope is observed. This is the case also in the experiment discussed in Sec. III C. Apparently, the cubic correction parameter  $a$  contributes to the slope to a much smaller extent.

Finally, it should be noted that finite values of the sheath potential during collapse can, in principle, be easily included. The individual sheath voltages can always be represented by a dynamic part, as is already done in the model, plus a constant which represents the finite value. In the balance only the difference of the two constants at both sheaths remains and can be combined with the self-bias. It is straightforward to show (for a Maxwellian distribution function) that the additional term is given by  $kT_e/(ek) \ln(\varepsilon)$  as long as  $\varepsilon \gg kT_e/(eV_0) \ll 1$ , where  $k$  in the denominator has been defined above. This term is always much smaller than the self-bias and does not change the sheath dynamics noticeably. However, the position  $\xi = 1$  now no longer represents the electrode surface but a position slightly in front of it and the total individual sheath voltages are the sum of the dynamic part discussed here and the constant representing the finite minimum.

### APPENDIX C: SCREENING FUNCTION AND OPTIMIZED VALUE OF THE EXPONENT $\nu$

The screening function  $g$  can be calculated numerically as outlined in Sec. II C. However, it is desirable to have an analytical expression available for the analytical solution of the sheath differential equation. A simple power law provides a convenient form for the fit as well as for further analytical calculations. Naturally, an ansatz with  $g = \xi^\nu$ , with  $0 < \nu < 1$  has all the characteristic properties found generally for  $g$ : It varies monotonously between zero and one in the range  $0 \leq \xi \leq 1$ , has a positively diverging derivate at zero, and shows a concave curvature throughout. The exponent can be determined from the numerical form of  $g$  by minimizing the

integral difference squared:

$$\frac{\partial}{\partial \nu} \int_0^1 [g(\xi) - \xi^\nu]^2 d\xi = 0. \quad (\text{C1})$$

This leads to the following transcendental equation for  $\nu$ :

$$2\nu + 1 = \frac{1}{\int_0^1 g(\xi) \ln(\xi) \xi^\nu d\xi}. \quad (\text{C2})$$

Fortunately, the right hand side varies effectively linearly with  $\nu$  in the relevant range  $0 < \nu < 1$  and can therefore be expanded in very good approximation to first order around  $\nu = 0$ . Alternatively, one could also expand around the centre of the interval at  $\nu = 0.5$ , which leads to a more complex final equation. However, the difference in the result for the optimized value of  $\nu$  is typically only about 1% so that the simpler alternative is preferred. With this linearization, the equation is easily solved for  $\nu$ :

$$\nu \approx \frac{2I_1(1 - \sqrt{I_1})}{4I_1^{3/2} - I_2}. \quad (\text{C3})$$

$I_1$  and  $I_2$  represent the following integrals:

$$I_1 = - \int_0^1 g(\xi) \ln(\xi) d\xi \quad \text{and} \quad I_2 = \int_0^1 g(\xi) \ln^2(\xi) d\xi. \quad (\text{C4})$$

Equation (C3) allows a fast and convenient calculation of the optimized exponent. For instance, in case of a simple linear scaling  $W \propto \xi$  (neglecting the boundary condition), which corresponds to a linear mean electric field, the scaling factor cancels out exactly when calculating the normalized sheath voltage  $v(\xi) = 1 - \tilde{v}(\xi)/\tilde{v}(1)$  and thereby via Eq. (18) also  $g(\xi)$ . By Eq. (C3) the optimized exponent follows as  $\nu = 0.338$ , a value close to the general choice of  $\nu = 0.375$ . Further, a typical example comparing the simple power law with the optimized exponent to the numerical solution of the sheath differential equation is given in Fig. 27 for the case  $\gamma = 60$  and  $\beta = 15$ , which gives  $\nu = 0.391$ . Excellent agreement between the numerically obtained form of  $g$  and the

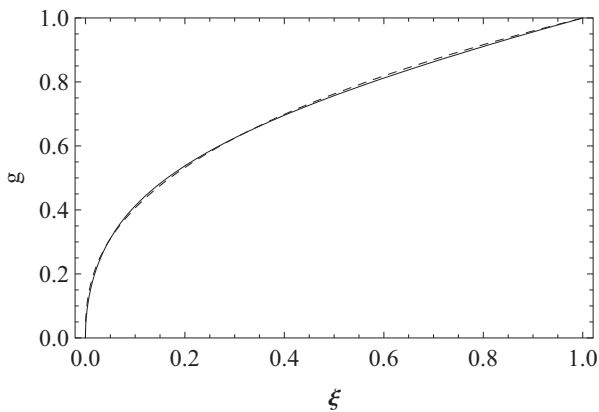


FIG. 27. Screening function  $g$  as determined numerically for  $\gamma = 60$  and  $\beta = 15$  (solid line) and the approximate analytical form  $g_a = \xi^\nu$  with an exponent of  $\nu = 0.391$ , optimized according to Eq. (C3) (dashed line). Both curves are effectively on top of each other.

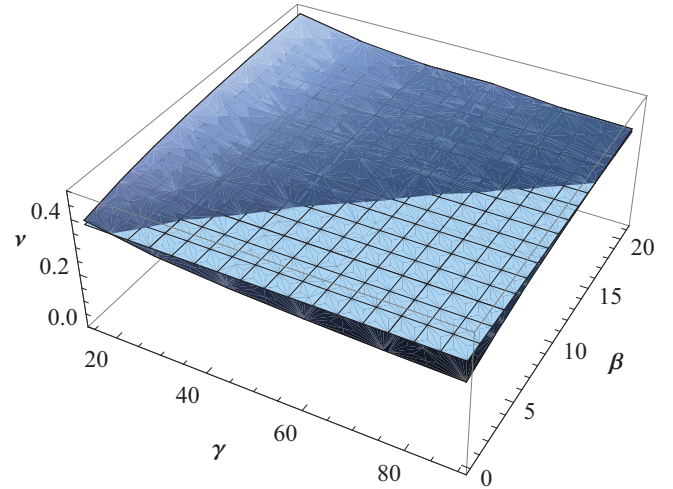


FIG. 28. (Color online) Exponent  $\nu$  for the simple power scaling approximation to the screening function  $g$  as function of the density parameter  $\gamma$  and the collision parameter  $\beta$ . The surface representing the values of  $\nu$  is semitransparent in order to allow comparison with the proposed universal exponent of  $\nu = 3/8$ , which is represented by a grid. The surface of the optimized  $\nu$  values intercepts with the grid at about the diagonal going from the left to the right hand corner.

fit is found not only for these particular parameters but also throughout the entire  $\gamma$  and  $\beta$  parameter range.

It should be noted that a similar procedure can also be applied in order to determine the exponent of the sinusoidal wave form approximating the sheath voltage by comparison with either experimental data, e.g., from capacitive probe measurements, or PIC simulation results. In this case  $g$  has to be replaced by the voltage and  $\xi$  by the absolute value of the sinus. However, then all integrals must be evaluated numerically.

The exponent is now determined within a wide and characteristic range of parameters  $\gamma$  and  $\beta$  and displayed in Fig. 28 together with the proposed universal exponent of  $\nu = 3/8$ . This figure demonstrates that, in fact, the exponent is varying only within a narrow range. In most cases the plasma density ( $\gamma$ ) increases with the neutral gas density ( $\beta$ ), which is represented by the diagonal where both planes intercept. Alternatively, the numerical surface could be approximated by some analytical function. However, the increase in complexity does not seem to be compensated by a similar gain in accuracy. In conclusion, in this work the exponent is set constant at a universal value of  $\nu = 3/8$ .

Finally, the sensitivity of this result on the particular choice of the universal value for  $\nu$  should be addressed briefly. For the characteristic parameter range discussed above one can write  $\nu = 3/8 \pm \Delta\nu$  with  $\Delta\nu \approx 0.05$ , where the minus sign applies for the collisionless case ( $\beta = 0$ ) and the plus sign for the collisional case ( $\beta \gg 1$ ). The analytical solutions for arbitrary values of  $\nu$  are

$$W(\xi) = \begin{cases} 1 + \left[ \frac{9\gamma^2 \xi^{2+\nu}}{2(2+\nu)(1+2\nu)} \right]^{2/3}, & \beta = 0, \\ \left[ 1 + \frac{3\gamma^2 \xi^{1+\nu}}{\beta^2(1+\nu)} \right]^{2/3}, & \beta \gg 1. \end{cases} \quad (\text{C5})$$

For large values of  $\gamma$  the initial value for  $W$  can be ignored already for rather small values of  $\xi$  and a simple power

law results for  $W$ . The exponents are  $(19 - 0.4)/12$  for the collisionless case and  $(11 + 0.4)/12$  for the collisional case with  $0.4 = 8\Delta v$ . Similarly, the maximum range for amplitude variation is only a few percent in both cases. Clearly, the effect of small variations in  $v$  is negligible. One could even argue that the effect would still be small for even larger variations, which explains partly the insensitivity of the final solution to variations in the screening function.

By combining the above general solution (C5) with Eqs. (16)–(18) for calculating  $g(\xi)$  and Eq. (C3) defining the optimum exponent  $\nu$ , this value can be determined self-consistently by using entirely the analytical solutions. Since the deviations from the self-consistent numerical solution is mainly caused by the use of the universal exponent this would lead to an improvement of the accuracy of the analytical solution. However, this concept is rather complicated and requires numerical integration while the accuracy is already quite satisfying using the universal value. Therefore, this option is not further investigated here.

#### APPENDIX D: APPROXIMATE SOLUTIONS FOR THE CHARGE AND VOLTAGE FUNCTIONS AND THE DYNAMIC SHEATH EDGE POSITION

The charge and voltage functions  $\tilde{q}(\xi)$  and  $\tilde{v}(\xi)$  [Eqs. (15) and (17)] are central for calculating all the derived sheath quantities like fields, current density, or the cubic correction parameter. In particular, they are also essential for calculating the dynamic sheath edge position  $\xi_s(\varphi)$ . The integrals defining these functions can be solved exactly in terms of the hypergeometric function [Eqs. (36), (37), (40), and (41)]. Nevertheless, for practical purposes it is desirable to express these integrals by more elementary functions. This can be realized in good approximation after some transformation and subsequent expansion of the integrals. The procedure is similar for all integrals. First the integrals are transformed into integrals with respect to  $W$ :

$$\tilde{q}[W(\xi)] = \begin{cases} \beta = 0: & \left(\frac{133}{144\gamma^2}\right)^{8/19} \frac{12}{19} \int_1^W \frac{dy}{y^{1/2}(y-1)^{7/19}}, \\ \beta \gg 1: & \frac{1}{\alpha^{8/11}} \frac{8}{11} \int_1^W \frac{W^{3/2}}{y^{1/3}(y-1)^{3/11}} dy, \end{cases} \quad (\text{D1})$$

$$\tilde{v}[W(\xi)] = \tilde{q}[W(\xi)] - \begin{cases} \beta = 0: & \left(\frac{133}{144\gamma^2}\right)^{16/19} \frac{12}{19} \int_1^W \frac{(y-1)^{5/19} dy}{y^{1/2}}, \\ \beta \gg 1: & \frac{1}{\alpha^{16/11}} \frac{8}{11} \int_1^W \frac{W^{3/2}}{y^{1/3}} \frac{(y-1)^{5/11} dy}{y^{1/3}}. \end{cases} \quad (\text{D2})$$

Now a partial integration is performed in order to remove the divergences at  $y = 1$  in Eqs. (D1) and the nominator of the remaining integral is expanded to first order in  $1/y$ . This generates two new integrals which can be solved elementarily:

$$\tilde{q}[W(\xi)] = \begin{cases} \beta = 0: & \left(\frac{133}{144\gamma^2}\right)^{8/19} \left[ \frac{(W-1)^{12/19}}{W^{1/2}} + \frac{19}{5}(W^{5/38} - 1) - \frac{4}{11}(W^{-33/38} - 1) \right], \\ \beta \gg 1: & \frac{1}{\alpha^{8/11}} \left[ \frac{(W^{3/2}-1)^{8/11}}{W^{1/2}} + \frac{11}{13}(W^{13/22} - 1) - \frac{11}{20}(W^{-10/11} - 1) \right], \end{cases} \quad (\text{D3})$$

$$\tilde{v}[W(\xi)] = \tilde{q}(W) - \frac{1}{2} \begin{cases} \beta = 0: & \left(\frac{133}{144\gamma^2}\right)^{16/19} \left[ \frac{(W-1)^{24/19}}{W^{1/2}} + \frac{19}{29}(W^{29/38} - 1) - \frac{19}{7}(W^{-7/38} - 1) \right], \\ \beta \gg 1: & \frac{1}{\alpha^{16/11}} \left[ \frac{(W^{3/2}-1)^{16/11}}{W^{1/2}} + \frac{11}{37}(W^{37/22} - 1) + \frac{11}{4}(W^{2/11} - 1) \right]. \end{cases} \quad (\text{D4})$$

Here the solutions are expressed as functions of  $W(\xi)$  rather than  $\xi$  in order to have a more compact representation. The approximate solutions have a very good accuracy. The error peaks around  $W = 1.1$ , i.e., at  $\xi \ll 1$ , with a value of about 6% and falls quickly off for larger values of  $W$  to about 1%. Further improvement of the accuracy could be achieved by using higher order expansion but the present accuracy should already be sufficient for all practical purposes within the frame of this work.

The straightforward way of calculating the dynamic sheath edge position  $\xi_s(\varphi)$  would be resolving  $v$ , respectively  $\tilde{v}$ , for  $W$  and then for  $\xi$ . However, neither Eq. (D3) nor Eq. (D4) can be solved analytically for  $W$ . Fortunately, the requirements on the precision are a little more relaxed for this calculation and a cruder approximation can be made. Since again the procedure is similar for the two extreme cases of collisionality, the calculations are carried out in parallel. First, the charge function  $\tilde{q}$  is expanded for large values of  $W$ , keeping only the leading term. This still gives a very good approximation for large values but fails naturally for low values of  $W$  closer to 1. Indeed, the expansions terminate at small but finite positive values. In order to ensure the correct value at the boundary  $\tilde{q}(W = 1) = 0$ , the asymptotic relations are *ad hoc* extended by appropriate constants of the order of one added to  $W$ . For  $\beta = 0$  this means  $W \rightarrow W - 1 + 0.878^{38/5}$  and for  $\beta \gg 1$  the extension is  $W \rightarrow (W^{3/2} - 1)^{2/3} - 0.692^{22/13}$ . This crude method introduces actually only a small error in determining  $\xi_s$  since the correction becomes noticeable only when  $\xi_s$  is close to zero anyway. However, it ensures proper convergence to this value. The resulting relations are

$$\tilde{q}(W) \approx \begin{cases} \beta = 0: & \frac{24}{5} [(W - 1 + 0.878^{38/5})^{5/38} - 0.878], \\ \beta \gg 1: & \frac{24}{13} \{ [(W^{3/2} - 1)^{2/3} + 0.692^{22/13}]^{13/22} - 0.692 \}. \end{cases} \quad (\text{D5})$$

These equations can be explicitly solved for  $W$ . Then  $W$  is solved for  $\xi$  using the analytical solutions for  $W$  [Eqs. (35) and (39)] and  $\tilde{q}$  is replaced by its relation to  $q$  [Eq. (14)] to determine  $\xi_s(q)$ . Since  $q$  can be expressed by the cubic charge-voltage relation [Eq. (20)] as a function of  $v$  and the sheath voltage  $v$  is again a known function of  $\varphi$ , one finally arrives at the desired result  $\xi_s(\varphi)$ .

After some algebraic rearrangements, one finds

$$\xi_s(\varphi) = \begin{cases} \beta = 0: & \left\{ \frac{(\kappa\{1-g[v(\varphi)]\}+1)^{38/5}-1}{(\kappa+1)^{38/5}-1} \right\}^{12/19}, \\ \beta \gg 1: & \left\{ \frac{(\kappa\{1-g[v(\varphi)]\}+1)^{22/13}-1}{(\kappa+1)^{22/13}-1} \right\}^{12/11}, \end{cases} \quad (\text{D6a})$$

$$\kappa = \begin{cases} \beta = 0: & (2.828\gamma^{4/3} + 1)^{5/38} - 1, \\ \beta \gg 1: & (1.864\alpha^{2/3} + 1)^{13/22} - 1. \end{cases} \quad (\text{D6b})$$

Comparison of Eqs. (D6) with parametric plots of the sheath edge position as a function of the rf phase, i.e., plotting  $\xi_s$  versus  $\varphi [v(\xi_s)]$ , with  $0 \leq \xi_s \leq 1$ , using the exact integrals shows excellent agreement for all parameters with undistinguishable curves on top of each other.

- 
- [1] M. A. Lieberman and A. J. Lichtenberg, *Principles of Plasma Discharges and Materials Processing*, 2nd ed. (Wiley & Sons, New York, 2005).
- [2] P. Chabert and N. St. J. Braithwaite, *Physics of Radio Frequency Plasmas* (Cambridge University Press, Cambridge, UK, 2011).
- [3] A. Metze, D. W. Ernie, and H. J. Oskam, *J. Appl. Phys.* **60**, 3081 (1986).
- [4] M. S. Barnes, T. J. Colter, and M. Elta, *J. Appl. Phys.* **61**, 81 (1987).
- [5] D. Graves, *J. Appl. Phys.* **62**, 88 (1987).
- [6] J. P. Boeuf, *Phys. Rev. A* **36**, 2782 (1987).
- [7] R. A. Gottscho, *Phys. Rev. A* **36**, 2233 (1987).
- [8] A. D. Richards, D. Thomson, and H. Sawin, *Appl. Phys. Lett.* **50**, 492 (1987).
- [9] K. U. Riemann, *J. Appl. Phys.* **65**, 999 (1989).
- [10] S. Biehler, *Appl. Phys. Lett.* **54**, 317 (1989).
- [11] M. A. Lieberman, *IEEE Trans. Plasma Sci.* **16**, 638 (1988).
- [12] M. A. Lieberman, *IEEE Trans. Plasma Sci.* **17**, 338 (1989).
- [13] M. A. Lieberman, *J. Appl. Phys.* **65**, 4186 (1989).
- [14] P. M. Vallinga and F. J. de Hoog, *J. Phys. D: Appl. Phys.* **22**, 925 (1989).
- [15] P. M. Vallinga, P. M. Meijer, and F. J. de Hoog, *J. Phys. D: Appl. Phys.* **22**, 1650 (1989).
- [16] K. O. Okazaki, T. Makabe, and Y. Yamaguchi, *Appl. Phys. Lett.* **54**, 1742 (1989).
- [17] Ch. Wild and P. Koidl, *Appl. Phys. Lett.* **54**, 505 (1989).
- [18] Chris M. Horwitz, T. Putzer, and A. M. Smith, *J. Vac. Sci. Technol. A* **8**, 3124 (1990).
- [19] Valery A. Godyak and Natalia Sternberg, *Phys. Rev. A* **42**, 2299 (1990).
- [20] Y. H. Oh, N. H. Choi, and D. I. Choi, *J. Appl. Phys.* **67**, 3264 (1990).
- [21] D. Vender and R. W. Boswell, *IEEE Trans. Plasma Sci.* **18**, 725 (1990).
- [22] S. K. Park and D. J. Economou, *J. Appl. Phys.* **68**, 3904 (1990).
- [23] P. Belenger and J. P. Boeuf, *Phys. Rev. A* **41**, 4447 (1990).
- [24] Karla Börnig, *Appl. Phys. Lett.* **60**, 1553 (1992).
- [25] J. P. Booth, J. Derouard, M. Fadlallah, and N. Sadeghi, *J. Appl. Phys.* **74**, 862 (1993).
- [26] K. E. Greenberg and G. A. Hebner, *Appl. Phys. Lett.* **63**, 3282 (1993).
- [27] M. D. Bowden, T. Nakamura, K. Muraoka, Y. Yamagata, B. W. James, and M. Maeda, *J. Appl. Phys.* **73**, 3664 (1993).
- [28] T. E. Nitschke and D. Graves, *J. Appl. Phys.* **76**, 5646 (1994).
- [29] Michael Klick, *J. Appl. Phys.* **79**, 3445 (1996).
- [30] M. E. Riley, Sandia Report SAND95-0775, UC-401, 1995.
- [31] M. E. Riley, Sandia Report SAND96-1948, UC-401, 1996.
- [32] M. J. Grapperhaus and M. J. Kushner, *J. Appl. Phys.* **81**, 569 (1997).
- [33] J. Gierling and K.-U. Riemann, *J. Appl. Phys.* **83**, 3521 (1998).
- [34] T. Panagopoulos and D. Economou, *J. Appl. Phys.* **85**, 3435 (1999).
- [35] E. Kawamura, V. Vahedi, M. A. Lieberman, and C. K. Birdsall, *Plasma Sources Sci. Technol.* **8**, R45 (1999).
- [36] M. A. Sobolewski, *Phys. Rev. E* **62**, 8540 (2000).
- [37] Z.-L. Dai, Y.-N. Wang, and T.-C. Ma, *Phys. Rev. E* **65**, 036403 (2002).
- [38] S. Roy, B. P. Pandey, J. Poggie, and D. V. Gaitonde, *Phys. Plasmas* **10**, 2578 (2003).
- [39] H. Kumar and S. Roy, *Phys. Plasmas* **12**, 093508 (2005).
- [40] M. M. Turner, *Phys. Plasma* **13**, 033506 (2006).
- [41] Z. Donko, *Plasma Sources Sci. Technol.* **20**, 024001 (2011).
- [42] Y. Wang, M. A. Lieberman, A. C. F. Wu, and J. P. Verboncoeur, *J. Appl. Phys.* **110**, 033307 (2011).
- [43] D.-C. Kwon, M.-Y. Song, and J.-S. Yoon, *J. Phys. D: Appl. Phys.* **46**, 025202 (2013).
- [44] M. M. Turner and P. Chabert, arXiv:1212.2612.
- [45] M. Kratzer, R. P. Brinkmann, W. Sabisch, and H. Schmidt, *J. Appl. Phys.* **90**, 2169 (2001).
- [46] B. G. Heil, R. P. Brinkmann, and U. Czarnetzki, *J. Phys. D: Appl. Phys.* **41**, 225208 (2008).
- [47] M. Shihab, D. Ziegler, and R. P. Brinkmann, *J. Phys. D: Appl. Phys.* **45**, 185202 (2012).
- [48] D. J. Economou, D. A. Evans, and R. C. Alkire, *J. Electrochem. Soc.: Solid State Science and Technology* **135**, 756 (1988).
- [49] K. U. Riemann, *Phys. Fluids B* **4**, 2693 (1992).
- [50] K. U. Riemann, *Phys. Plasmas* **4**, 4158 (1997).
- [51] R. P. Brinkmann, *J. Appl. Phys.* **102**, 093303 (2007).
- [52] R. P. Brinkmann, *J. Phys. D: Appl. Phys.* **42**, 194009 (2009).
- [53] G. Gozandinos, M. M. Turner, and D. Vender, *Phys. Rev. Lett.* **87**, 135004 (2001).
- [54] I. D. Kagarnovich, O. V. Polomarov, and C. E. Theodosiou, *IEEE Trans. Plasma Sci.* **34**, 696 (2006).
- [55] E. Kawamura, M. A. Lieberman, and A. J. Lichtenberg, *Phys. Plasmas* **13**, 053506 (2006).

- [56] M. M. Turner, *J. Phys. D: Appl. Phys.* **42**, 194008 (2009).
- [57] U. Czarnetzki, D. Luggenhölscher, and H. F. Döbele, *Plasma Sources Sci. Technol.* **8**, 230 (1999).
- [58] U. Czarnetzki, D. Luggenhölscher, and H. F. Döbele, *Appl. Phys. A* **72**, 509 (2001).
- [59] U. Czarnetzki, T. Mussenbrock, and R. P. Brinkmann, *Phys. Plasmas* **13**, 123503 (2006).
- [60] J. Schulze, B. G. Heil, D. Luggenhölscher, R. P. Brinkmann, and U. Czarnetzki, *J. Phys. D: Appl. Phys.* **41**, 195212 (2008).
- [61] B. G. Heil, U. Czarnetzki, R. P. Brinkmann, and T. Mussenbrock, *J. Phys. D: Appl. Phys.* **41**, 165202 (2008).
- [62] U. Czarnetzki, J. Schulze, E. Schüngel, and Z. Donko, *Plasma Sources Sci. Technol.* **20**, 024010 (2011).
- [63] J. Schulze, E. Schüngel, Z. Donko, and U. Czarnetzki, *J. Phys. D: Appl. Phys.* **43**, 225201 (2010).
- [64] R. P. Brinkmann, *J. Phys. D: Appl. Phys.* **44**, 042002 (2011).
- [65] F. Tochikubo, A. J. Suzuki, S. Kakuta, Y. Terazono, and T. Makabe, *Appl. Phys.* **68**, 5532 (1990).
- [66] C. M. O. Mahony, R. Al Wazan, and W. G. Graham, *Appl. Phys. Lett.* **71**, 608 (1997).
- [67] A. E. Elgendy, H. Hatefinia, T. Hemke, M. Shihab, A. Wollny, D. Eremin, T. Mussenbrock, and R. P. Brinkmann, arXiv:1306.1664.
- [68] K. S. Govinder and P. G. L. Leach, *J. Nonlinear Math. Phys.* **14**, 443 (2007).
- [69] P. J. Hargis, K. E. Greenberg, P. A. Miller *et al.*, *Rev. Sci. Instrum.* **65**, 140 (1994).
- [70] J. Schulze, Z. Donko, B. G. Heil, D. Luggenhölscher, T. Mussenbrock, R. P. Brinkmann, and U. Czarnetzki, *J. Phys. D: Appl. Phys.* **41**, 105214 (2008).
- [71] T. Simko, V. Martisovits, J. Bretagne, and G. Gousset, *Phys. Rev. E* **56**, 5908 (1997).
- [72] K.-U. Riemann, *J. Phys D: Appl. Phys.* **24**, 493 (1991).
- [73] W. H. Cramer and J. H. Simons, *J. Chem. Phys.* **26**, 1272 (1957).
- [74] J. S. W. Wong, *SIAM Rev.* **17**, 339 (1975).
- [75] J. Schulze, Ph.D. thesis, Ruhr University Bochum, 2009, <http://www-brs.ub.ruhr-uni-bochum.de/netathtml/HSS/Diss/SchulzeFelixJulian/diss.pdf>.
- [76] M. L. Hause, B. D. Prince, and R. J. Bernish, *J. Appl. Phys.* **113**, 163301 (2013).
- [77] J. E. Lawler, *Phys. Rev. A* **32**, 2977 (1985).
- [78] G. H. Wannier, *Statistical Physics* (Wiley & Sons, New York, 1966).
- [79] T. Mussenbrock, R. P. Brinkmann, M. A. Lieberman, A. J. Lichtenberg, and E. Kawamura, *Phys. Rev. Lett.* **101**, 085004 (2008).